CHARACTERIZING THE FUNCTION OF MON1A IN MEMBRANE TRAFFIC AND ORGANELLE MAINTENANCE IN THE SECRETORY PATHWAY

by

Dustin C. Bagley

A dissertation submitted to the faculty of
The University of Utah
in partial fulfillment of the requirements for the degree of

Doctor of Philosophy

in

Microbiology and Immunology

Department of Pathology

The University of Utah

August 2013

THE UNIVERSITY OF UTAH GRADUATE SCHOOL

STATEMENT OF DISSERTATION APPROVAL

The dissertation of Dustin C. Bagley,

has been approved by the following supervisory committee members:

Jerry Kaplan, Chair	5-14-2013	Date Approved
Diane McVey-Ward, Member	5-14-2013	Date Approved
Janis Weis, Member	5-20-2013	Date Approved
David Stillman, Member	5-14-2013	Date Approved
Wesley Sundquist, Member	5-15-2013	Date Approved

and by Peter Jensen, Chair of

the Department of Microbiology and Immunology

and by Donna M. White, Interim Dean of The Graduate School.

ABSTRACT

Mon1 is an evolutionarily conserved gene that has homologs from yeast to humans. The original identification and characterization of Mon1 in mammals, Mon1a, was performed in a study that identified Mon1a as a modifier of iron homeostasis in mice. That work demonstrated that C57BL mice harbor an intrinsic "gain-of-function" mutation that resulted in an excess of the iron exporter ferroportin at the cell surface of iron recycling macrophages. The study also showed that Mon1a had a function in the movement of soluble and membrane-bound proteins through the secretory apparatus. We were able to expand on those findings using protein interaction and RNAi analysis to demonstrate that Mon1a associates with the molecular motor Dynein, known to function in ER-Golgi trafficking. Subcellular localization demonstrated that Mon1a peripherally associates with the ER membrane. Further, RNAi-mediated reduction of Mon1a resulted in a significant decrease in the formation of ER-derived vesicle, which resulted in impaired trafficking in the early secretory pathway. We also determined that the movement of the viral protein VSVGtsGFP from the Golgi to the plasma membrane was delayed in Mon1a-depleted cells.

A yeast two-hybrid (Y2H) analysis of Mon1a interacting partners found that a F-BAR domain-contain protein, FCHo2, known to affect membrane traffic at the cell surface, physically associated with Mon1a. RNAi-mediate reduction of Mon1a or

FCHo2 resulted in severe Golgi fragmentation, which was dependent on the activity of the Golgi GTPase Rab6. The RNAi-mediate phenotypes of Mon1a and FCHo2 were not identical as only FCHo2 silencing-induced Golgi fragmentation was cell cycle-dependent. We show using FRAP analysis that FCHo2 is necessary for the lateral movement of membrane proteins between Golgi elements that link Golgi cisternae. We determined that FCHo2-mediated Golgi fragmentation resulted in immature glycosylation moieties at the plasma membrane. This dissertation describes novel roles for both Mon1a and FCHo2 in membrane traffic in the secretory pathway and Golgi architecture maintenance.

To my family Brittany, Ann, and Barry

CONTENTS

LIST OF FIGURES

ACKNOWLEDGEMENTS

I have to begin by thanking my family. My sister, Brittany, and my parents, Ann and Barry, gave me all the support and strength I needed that allowed this work to be completed. I am eternally grateful for them now and always.

I would like to thank my mentors, Jerry Kaplan and Diane Ward, who over the years have made me a better scientist. I am grateful for all the time they spent shaping me into the young scientist I am today. I am a better researcher because of them.

I would like to recognize my committee members, who always made time to discuss my science. My research reaped the benefits of their guidance and expertise and I am grateful for all the effort and discussions they allowed me.

CHAPTER 1

INTRODUCTION

A unique and unifying characteristic of all eukaryotes is the evolution of intracellular compartmentalization. The development of an elaborate endomembrane system has allowed for the separation of many biochemical processes, giving rise to sophisticated temporal and spatial regulation that is absent in prokaryotes (1-5). A representative example of this is the separation that can be seen with protein synthesis in the endoplasmic reticulum and protein glycosylation within the Golgi apparatus. The secretory and endocytic pathways of the endomembrane system are responsible for maintaining the size and shape of the cell. The biosynthetic pathway is responsible for the synthesis and secretion of cytokines, hormones, antibodies, growth factors, receptors, ligands, and thousands of other cargoes. Molecular machinery estimated at more than 2000 proteins is required to insure fidelity and functionality of the endomembrane system (1,2,4,6). Disruption of this machinery through genetic alteration or other means results in disease. Diseases ranging from Chediak-Higashi to schizophrenia and cranio-lenticulo-sutural dysplasia (CLSD) result from membrane traffic breakdown (7,8). Understanding how organelles retain their identity and functionality despite continuous

regulated transport of proteins and lipids between these intracellular compartments has been a central question in cell biology.

The anatomy of the endomembrane system was first described at the turn of the 19th century when the Italian histologist Camillo Golgi identified an intracellular tubular structure using silver nitrate-based cytochemical staining to study the central nervous system (9,10). The Golgi apparatus became the first endomembrane compartment identified. Elie Metchnikoff, a contemporary of Golgi, demonstrated that individual cells possess machinery that allowed them to internalize extracellular material in a process that has since been termed endocytosis (9,11,12). Biologists at this time were beginning to appreciate the nature of these intracellular membrane-bound organelles; however, it would be nearly another century before techniques were developed to define the enormity and complexity of the endomembrane system and regulatory machinery.

In the mid-1900s seminal work by Palade, de Duve, and Novikoff using cell fractionation, enzymatic assays, and electron microscopy provided the critical insight that these membrane-bound intracellular compartments were sites of distinct biochemical functions (9). Palade identified components of the mammalian endomembrane system by mapping the secretory pathway by pulse-chase autoradiographic tracing of zymogen enzyme in pancreatic tissue (9,13-15). This work revealed directionality to the biosynthetic pathway. Newly synthesized proteins in the ER are trafficked in vesicle intermediates to the Golgi apparatus to be matured and sorted. Mature proteins leave the Golgi in secretory vesicles, ultimately reaching the plasma membrane (PM) for release of their content into the extracellular milieu. This novel insight of ER to Golgi to PM trafficking became the cell biology equivalent to the molecular biology axiom: DNA to

RNA to protein. Palade and colleagues framed the ultrastructural identity of the secretory and endocytic apparatuses; however, development of new techniques and technologies were necessary to uncover the molecular machinery required to regulate these complex intracellular pathways.

Another critical observation stemming from the Palade laboratory was the fundamental principle that organelles communicate with their downstream counterpart through membrane-bound vesicle transport intermediates (16,17). Further, for every forward (anterograde) trafficking step in the endomembrane system, a recycling (retrograde) trafficking event occurs that preserves the integrity of organelle composition and function (18-21). Modern techniques including cell-free *in vitro* reconstitution assays, use of model organisms and genetic screens in conjunction with classical protocols of subcellular fractionation, and ultrastructural analysis began to define the complexity of the machinery required to regulate intracellular membrane trafficking. In an elegant genetic screen using the budding yeast *Saccharomyces cerevisiae,* Randy Schekman and Peter Novick identified many of the molecular components required at the initial trafficking step of the secretory pathway, many of which have mammalian homologs (22-24).

The focus of the work discussed in this thesis is the characterization of Mon1a, the mammalian homolog of yeast Mon1. Mon1a was originally identified in a quantitative trait locus (QTL) analysis in mice designed to identify modifier genes of iron homeostasis (25).

1.1 Identification of Mon1a: a membrane traffic regulator that affects iron metabolism

Iron is an element essential in nearly all organisms because of its facile ability to gain and lose electrons, which is a process required in numerous biochemical processes (26,27). For the same reason that iron can be beneficial, it also can be harmful at high concentrations. Organisms must tightly regulate intracellular iron levels. When this regulation breaks down, disease occurs. Excessive tissue iron deposition is called hemochromatosis, which in humans has a highly variable clinical outcome. Hemochromatosis is a recessive disorder that arises due to mutations in a limited number of iron regulatory genes. The variability in patient disease progression is likely the result of many genes modifying the outcome of iron overload (28). In a QTL analysis, Mon1a was identified as a modifier of iron stores in different strains of mice (25).

Spleen iron content is largely supplied by macrophages that recycle iron from senescent red blood cells. Spleen iron levels vary minimally between mice of the same sex and age but not between strains of mice. Thus, spleen iron content was the trait followed in the QTL analysis. C57BL and SWR mice were used for the QTL analysis as they had the lowest and highest spleen iron levels, respectively. Ultimately, a single amino acid substitution was identified in an evolutionarily conserved residue (N374S) in the Mon1a allele unique to C57BL mice.

Splenic iron levels are largely regulated by ferroportin, the only known mammalian iron exporter, and the mammalian Mon1a allele in C57BL macrophages results in significantly more ferroportin at the plasma membrane compared to SWR macrophages (25). Excessive cell surface ferroportin expression is accompanied by a decrease in intracellular iron and changes in ferroportin localization provided a logical

explanation for the differences observed in spleen iron content in these two mice strains. Depletion of Mon1a protein in bone marrow-derived macrophages using siRNA tested this hypothesis. Decreased Mon1a protein led to a significant reduction in plasma membrane ferroportin and a concomitant increase in intracellular iron. These results demonstrated that altering Mon1a levels affected cellular iron metabolism and accounted for the differences between C57BL and SWR mice spleen iron content.

Mon1a clearly affects the localization of ferroportin and ultimately iron metabolism but what was unclear was if Mon1a function was specific to iron regulation or was it more global. Indeed, Mon1a silencing resulted in significant reduction in secretion of IL-12, IL-6, MIF, and other molecules, demonstrating that Mon1a regulated the movement of soluble and membrane-bound proteins through the secretory apparatus. This study suggested that the C57BL mice strain harbored an intrinsic "gain-of-function" Mon1a allele, which regulated the rate of traffic through the secretory apparatus.

1.2 Identification of Mon1 in yeast

Selective cargo recruitment and faithful targeting of transport vesicles to accepting compartments preserves organelle identity and functionality by preventing homogenization of endomembrane compartments (2,5,29). Studies in *S. cerevisiae* identified many components required for efficient bidirectional trafficking in the exo- and endocytic pathways (22-24,30). Central to the endocytic pathway in yeast is the vacuole that houses many biochemical processes affecting cellular physiology, organelle turnover, and protein degradation. The vacuole is subjected to constant fission and fusion events that must be tightly regulated. When gene products involved in this regulation

become disrupted, vacuolar fidelity and maintenance of morphology break down. Analysis of a gene deletion library revealed Mon1 and another protein, Ccz1, are required for proper trafficking to the vacuole as well as maintaining vacuole architecture (30,31).

Material enters the vacuole through a number of regulated pathways including autophagy, the multivesicular body (MVB) pathway, and the secretory pathway. Certain hydrolases, including soluble aminopeptidase I (Ape1), that reside in the vacuole, traffic through the cytoplasm to vacuole targeting (Cvt) pathway as immature peptides and are then cleaved into their mature form in the acidic environment of the vacuole. Importantly, processes and machinery required in the Cvt pathway overlap with those of autophagy and other trafficking events (30). To gain insight into these processes, a yeast gene deletion library was screened to identify mutants with defects in Ape1 maturation. Two gene products, Mon1 and Ccz1, which had previously not been implicated in these pathways, were found to be required for Cvt/autophagy-based vacuolar import (30,31).

Genetic, biochemical, and morphological analysis revealed a role for Mon1 and Ccz1 in fusion at the vacuole. Mon1 forms a stable complex with Ccz1 and the complex is recruited to the vacuole where it peripherally associates with the membrane. Deletion of Mon1 or Ccz1 disrupts membrane localization of the other protein and subsequently its function. In the absence of Mon1 or Ccz1, all membrane traffic that terminates at the vacuole (e.g. autophagy, Cvt, MVB, CPY pathways) is defective at the step of vacuolar fusion. Yeast strains lacking Mon1 or Ccz1 present with fragmented vacuoles, missorted vacuolar hydrolases (e.g. CPY), and are sensitive to high zinc concentrations (30-33). Mon1 and Ccz1 are required for homotypic vacuole fusion and function as a component of a *cis*-SNARE complex, which results in vacuole fragmentation when either protein is

deleted in yeast. Further work suggested that the Mon1-Ccz1 complex acts as a guanine nucleotide exchange factor (GEF), activating the late endosomal GTPase Ypt7, which is required for docking and fusion.

1.3 The role of SAND-1/Mon1a/b in the endocytic pathway

Mon1 is evolutionarily conserved and is found in all organisms from yeast to humans. There is only a single copy of Mon1 in yeast and *C. elegans*, yet there are two vertebrate homologues, Mon1a and Mon1b. Mon1 was originally characterized in yeast and its role was defined in the endocytic pathway. Understanding the function of Mon1 in the endocytic pathway of higher eukaryotes was the focus of recent studies, which revealed a requirement for Mon1, specifically in the maturation of the endosomal compartment (34-36).

Genetic and cell biological studies in *C. elegans* were done to analyze the role of the nematode homolog of Mon1, SAND-1 (36,37). *or552* is a temperature-sensitive mutation of SAND-1. *or552* is embryonic-lethal because it harbors a lesion in SAND-1, which is named after an evolutionarily conserved domain (the SAND domain) of unknown function. These *or552* mutant worms presented with an accumulation of granules in oocytes and coelomocytes. The granules originated from the endosomal pathway and were of both early and late endosomal origins. The study demonstrated that SAND-1 was a cytosolic protein peripherally associated with membranes of the early and late endocytic compartments. Further, SAND-1 was required for the membrane localization of the small Rab family GTPase Rab7. Rab7 function is required for the maturation of early to late endosomes. Interestingly, though SAND-1 was needed for the

transition at early to late endosomes, SAND-1 is not required at lysosomes despite its role in yeast. The authors claimed that Mon1 is functionally conserved from yeast to worms because SAND-1 is able to partially rescue *Δmon1* strains, despite functioning in distinct cellular environments.

Further studies in *C. elegans* showed that SAND-1 was required for the lysosomal degradation of engulfed apoptotic cells. Use of a *sand-1 (ok1963)* deletion mutant or RNAi against *sand-1* revealed an increase in the number of refractile bodies, condensed apoptotic cells found in the gonads of these worms. Refractile bodies stained brightly with acidic markers acridine orange and LysoTracker in the *sand-1* mutant, suggesting that apoptotic cells were internalized and acidified without impairment yet were defective later in the process of phagosomal maturation. The investigators posited that Mon1a function is evolutionarily conserved because clearance of apoptotic cells was rescued to wild type levels when mammalian Mon1a was expressed in the *sand-1* mutants. After cell corpse internalization, phagosomes mature from a $Rab5^+$ to a $Rab7^+$ compartment and in the absence of SAND-1 there was an increase in $Rab5^+$ phagosomes with a concomitant decrease of $Rab7^+$ phagosomes. Mechanistically, SAND-1/Mon1 affects Rab5 activation and downstream recruitment of Rab7, transitioning phagosomes to a more mature phenotype by removing the negative regulator of Rab7, a GDP dissociation inhibitor (GDI) (34).

Studies in mammalian cells showed that the mammalian Mon1 homologs also played a role in endosomal maturation. HeLa cells treated with siRNA oligos specifically targeted to Mon1a and Mon1b demonstrated an increase in the size of $Rab5^+$ endosomes, similar to *C. elegans*, but not in cells treated with siRNA oligos to either Mon1a or

Mon1b alone (35). Rab5 is activated through a GEF Rabex5, which was displaced through the overexpression of both Mon1a/b. Notably, Mon1b, but not Mon1a, interacted with the HOPS complex, which is known to recruit and activate Rab7 through GEF activity. This work demonstrated that SAND-1/Mon1b functions in the conversion of early ($Rab5^+$) to late ($Rab7^+$) endosomes by displacing Rabex5, the activator of Rab5, thus disrupting a positive feedback loop, recruitment, and activation of Rab7, likely through an interaction with the Rab7 GEF, the HOPS complex (35).

These studies demonstrated a role for Mon1 in the endocytic pathway, specifically in the maturation of early- to late- endosomes. Mon1 is evolutionarily conserved but the two vertebrate homologues (Mon1a and b) share less than 50% identity. Much of the work on Mon1 function in the endocytic pathway of mammalian cells focused on the role of Mon1b and much less on Mon1a (34,35). Also, these studies ignored the fact that mammalian Mon1a was originally identified as a regulator of membrane trafficking in the secretory pathway. None of the work published on Mon1 excludes it from functioning in the biosynthetic pathway and therefore, the aim of this thesis is to understand Mon1a activity, specifically in the mammalian secretory pathway. A short overview of the steps required for trafficking in the early secretory pathway are discussed below.

1.4 ER-derived vesicle formation

It is estimated that one third of the proteome is synthesized and packaged for transport at the ER, the initial step of membrane trafficking in the secretory pathway (1,5,29). Newly synthesized proteins are recruited and concentrated into ER-derived secretory vesicles at specialized structures known as ER exit sites (ERES). Cargo

recruitment and vesicle formation at ERES occurs via the sequential recruitment of the cytosolic proteins collectively known as the coat protein complex II (COPII). COPII proteins were originally identified in the Schekman *S. cerevisiae* genetic screen and are highly conserved in all eukaryotes (22-24).

COPII coat formation is initiated by the activation of the small GTPase Sar1 through a nucleotide exchange factor, Sec12, which activates Sar1. Activated Sar1 is recruited to the ERES membrane via insertion of an amphipathic α-helix, which creates membrane curvature while recruiting the heterodimeric Sec23-24 complex ("inner coat") that forms a concave, basic surface that is thought to stabilize and/or induce membrane curvature. The "outer coat" is subsequently recruited and is the product of another heterodimer complex, Sec13-31, which is believed to stabilize curvature and coat assembly as well as aid in vesicle scission, though the precise mechanism remains unclear (38,39). These five coat proteins have been demonstrated to be the minimal unit sufficient for vesicle formation using *in vitro* liposome-based assays; however, how vesicles are released and trafficked downstream to the intermediate compartment *in vivo* is still not fully understood.

Microtubules (MT) and the microtubule-based molecular motor Dynein are required for efficient ER to Golgi transport (40). Exactly how they function at a mechanistic level in vesicle formation and trafficking at the ER remains an open question. Several studies demonstrate that cargo is trafficked to the ER-Golgi intermediate compartment (ERGIC) in the presence of MT depolymerizing agents, suggesting that this initial transport step is MT-independent. Conversely, other studies show convincingly that ERES associate with MTs, and further, a subunit of the Dynein-

dynactin motor, Bicaudal-D (BICD1), interacts with the COPII inner coat protein Sec23 (20). Inhibiting this interaction delays vesicle trafficking to the Golgi apparatus, demonstrating that despite the significant strides to understanding vesicle trafficking at the early anterograde pathway, much remains to be elucidated. How Mon1a function is involved at this early stage of secretion is the topic of Chapter 2.

1.5 References

1. Gurkan, C., Koulov, A. V., and Balch, W. E. 2007 *Adv Exp Med Biol* 607: 73-83
2. Elias, M. 2010 *Mol Membr Biol* 27: 469-489
3. Lippincott-Schwartz, J., and Phair, R. D. 2010 *Annu Rev Biophys* 39: 559-578
4. Brighouse, A., Dacks, J. B., and Field, M. C. 2010 *Cell Mol Life Sci* 67: 3449-3465
5. Dacks, J. B., and Field, M. C. 2007 *J Cell Sci* 120: 2977-2985
6. Schekman, R. 2010 *Mol Biol Cell* 21: 3781-3784
7. Olkkonen, V. M., and Ikonen, E. 2006 *J Cell Sci* 119: 5031-5045
8. De Matteis, M. A., and Luini, A. 2011 *N Engl J Med* 365: 927-938
9. Mellman, I., and Warren, G. 2000 *Cell* 100: 99-112
10. Pannese, E. 1996 *Brain Res Bull* 41: 343-349
11. Heifets, L. 1982 *J Reticuloendothel Soc* 31: 381-391
12. Tauber, A. I. 1992 *Cell Immunol* 139: 505-530
13. Jamieson, J. D., and Palade, G. E. 1967 *J Cell Biol* 34: 597-615
14. Jamieson, J. D., and Palade, G. E. 1966 *Proc Natl Acad Sci U S A* 55: 424-431
15. Redman, C. M., Banerjee, D., Howell, K., and Palade, G. E. 1975 *Ann N Y Acad Sci* 253: 780-788

16. Castle, J. D., Jamieson, J. D., and Palade, G. E. 1972 *J Cell Biol* 53: 290-311

17. Kern, H. F., Jamieson, J. D., and Palade, G. E. 1972 *Verh Anat Ges* 67: 501-505

18. Del Nery, E., Miserey-Lenkei, S., Falguieres, T., Nizak, C., Johannes, L., Perez, F., and Goud, B. 2006 *Traffic* 7: 394-407

19. Feinstein, T. N., and Linstedt, A. D. 2008 *Mol Biol Cell* 19: 2696-2707

20. Matanis, T., Akhmanova, A., Wulf, P., Del Nery, E., Weide, T., Stepanova, T., Galjart, N., Grosveld, F., Goud, B., De Zeeuw, C. I., Barnekow, A., and Hoogenraad, C. C. 2002 *Nat Cell Biol* 4: 986-992

21. Young, J., Stauber, T., del Nery, E., Vernos, I., Pepperkok, R., and Nilsson, T. 2005 *Mol Biol Cell* 16: 162-177

22. Novick, P., Field, C., and Schekman, R. 1980 *Cell* 21: 205-215

23. Novick, P., Ferro, S., and Schekman, R. 1981 *Cell* 25: 461-469

24. Novick, P., and Schekman, R. 1979 *Proc Natl Acad Sci U S A* 76: 1858-1862

25. Wang, F., Paradkar, P. N., Custodio, A. O., McVey Ward, D., Fleming, M. D., Campagna, D., Roberts, K. A., Boyartchuk, V., Dietrich, W. F., Kaplan, J., and Andrews, N. C. 2007 *Nat Genet* 39: 1025-1032

26. Kaplan, J. 2002 *Cell* 111: 603-606

27. Kaplan, J., and O'Halloran, T. V. 1996 *Science* 271: 1510-1512

28. De Domenico, I., Ward, D. M., and Kaplan, J. 2011 *Semin Liver Dis* 31: 272-279

29. Vellai, T., and Vida, G. 1999 *Proc Biol Sci* 266: 1571-1577

30. Wang, C. W., Stromhaug, P. E., Shima, J., and Klionsky, D. J. 2002 *J Biol Chem* 277: 47917-47927

31. Wang, C. W., Stromhaug, P. E., Kauffman, E. J., Weisman, L. S., and Klionsky, D. J. 2003 *J Cell Biol* 163: 973-985

32. Bagley, D. C., Paradkar, P. N., Kaplan, J., and Ward, D. M. 2012 *The Journal of biological chemistry* 287: 25577-25588

33. Nordmann, M., Cabrera, M., Perz, A., Brocker, C., Ostrowicz, C., Engelbrecht-Vandre, S., and Ungermann, C. 2010 *Curr Biol* 20: 1654-1659

34. Kinchen, J. M., and Ravichandran, K. S. 2010 *Nature* 464: 778-782

35. Poteryaev, D., Datta, S., Ackema, K., Zerial, M., and Spang, A. 2010 *Cell* 141: 497-508

36. Poteryaev, D., Fares, H., Bowerman, B., and Spang, A. 2007 *EMBO J* 26: 301-312

37. Poteryaev, D., and Spang, A. 2005 *Biochem Soc Trans* 33: 606-608

38. Spang, A. 2009 *Curr Opin Cell Biol* 21: 531-536

39. Jin, L., Pahuja, K. B., Wickliffe, K. E., Gorur, A., Baumgartel, C., Schekman, R., and Rape, M. 2012 *Nature* 482: 495-500

40. Palmer, K. J., Hughes, H., and Stephens, D. J. 2009 *Mol Biol Cell* 20: 2885-2899

CHAPTER 2

MON1A PROTEIN ACTS IN TRAFFICKING THROUGH THE SECRETORY APPARATUS

Reproduced with permission from
Dustin C. Bagley, Prasad N. Paradkar, Jerry Kaplan, and Diane M. Ward.
June 4, 2012. Journal of Biological Chemistry DIO 10.1074/jbcM112354043

Mon1a Protein Acts in Trafficking through the Secretory Apparatus*[S]

Received for publication, February 21, 2012, and in revised form, May 7, 2012 Published, JBC Papers in Press, June 4, 2012, DOI 10.1074/jbc.M112.354043

Dustin C. Bagley[1], **Prasad N. Paradkar**[2], **Jerry Kaplan, and Diane M. Ward**[3]

From the Department of Pathology, School of Medicine, University of Utah, Salt Lake City, Utah 84132

Background: Mon1a is known to be involved in membrane trafficking.
Results: Reductions in Mon1a delay ER-to-Golgi trafficking and ERGIC-53-positive vesicle formation. Mon1a interacts with cytoplasmic dynein to efficiently traffic vesicles from ER to Golgi.
Conclusion: Mon1a plays a role in anterograde trafficking in the secretory pathway.
Significance: This work elucidates a role for Mon1a, known to be involved in the endocytic pathway, acting in the secretory pathway.

Mon1a was originally identified as a modifier gene of vesicular traffic, as a mutant Mon1a allele resulted in increased localization of cell surface proteins, whereas reduced levels of Mon1a showed decreased secretory activity. Here we show that Mon1a affects different steps in the secretory pathway including endoplasmic reticulum-to-Golgi traffic. siRNA-dependent reduction of Mon1a levels resulted in a delay in the reformation of the Golgi apparatus after Brefeldin A treatment. Endoglycosidase H treatment of ts045VSVG-GFP confirmed that knockdown of Mon1a delayed endoplasmic reticulum-to-Golgi trafficking. Reductions in Mon1a also resulted in delayed trafficking from Golgi to the plasma membrane. Immunoprecipitation and mass spectrometry analysis showed that Mon1a associates with dynein intermediate chain. Reductions in Mon1a or dynein altered steady state Golgi morphology. Reductions in Mon1a delayed formation of ERGIC-53-positive vesicles, whereas reductions in dynein did not affect vesicle formation. These data provide strong evidence for a role for Mon1a in anterograde trafficking through the secretory apparatus.

Membrane trafficking pathways in eukaryotes require highly regulated transfer of vesicles and their contents from a donor to an acceptor compartment. Mon1 was initially identified in *Saccharomyces cerevisiae* (YMon1)[4] as a protein required for vacuolar fusion. YMon1 acts as part of a *cis*-SNARE complex with Ccz1, and both are required in all pathways where the terminal compartment is the vacuole (1–3). Yeast with a deletion in *MON1* or its partner *CCZ1* have fragmented vacuoles resulting from a defect in vacuole fusion (1, 4). The *Caenorhabditis elegans* homologue of Mon1 (SAND-1) was shown to function in the endocytic pathway, although not at lysosomes but rather at early-to-late endosome maturation (5, 6). Mammalian Mon1 (Mon1a) and its homologue Mon1b were shown in both *C. elegans* and cultured mammalian cells to be involved in ingestion of apoptotic cell corpses (7). Recently, it was reported that Mon1a and Mon1b and the *C. elegans* homologue SAND-1 are involved in the Rab5-to-Rab7-mediated transition of endosomes (8). Studies in mammals utilized RNAi against both Mon1a and Mon1b to observe changes in the endocytic pathway, but no effects on the secretory pathway were reported.

The first identification of mammalian Mon1a suggested that it plays a role in the movement of molecules through the secretory apparatus (9). In that study, *Mon1a* was identified in a quantitative trait locus analysis for modifier genes of iron homeostasis. A missense mutation in the *Mon1a* gene in C57BL/6 mice gives rise to a single amino acid substitution (N374S) at an evolutionarily conserved residue. This substitution results in a "gain-of-function" allele causing an increase in the trafficking of membrane and soluble molecules through the biosynthetic pathway and thus increased localization of proteins at the plasma membrane. Reduction of Mon1a protein by RNAi supports the hypothesis that Mon1a plays a role in the trafficking of newly synthesized proteins through the secretory apparatus. In this study, we show that Mon1a functions in multiple steps in the secretory process including ER-to-Golgi traffic. We show that Mon1a interacts with cytoplasmic dynein and provide evidence that both are required for efficient anterograde trafficking from ER to Golgi.

EXPERIMENTAL PROCEDURES

Mammalian Cells and Constructs—NIH3T3, HeLa, Cos-7, and HeLa cells stably expressing GalNAc-T2-GFP were maintained in DMEM with 10% FBS plus or minus 0.4 g/liter G418 (Sigma-Aldrich). GalNAc-T2-GFP HeLa cells were a generous gift from Dr. Brian Storrie (University of Arkansas). pVSVG-GFP and ts045VSVG-GFP were a generous gift from Dr. Jennifer Lippincott-Schwartz (National Institutes of Health). Mouse Mon1a was cloned into pCMV-Tag2BFLAG (Stratagene, La

* This work was supported, in whole or in part, by National Institutes of Health Grant HL26922 (to D. M. W.).
[S] This article contains supplemental Figs. 1–4.
[1] Supported by National Institutes of Health Training Grant T32DK00715.
[2] Present address: Duke-National University of Singapore Graduate Medical School, 2 Jalan Bukit Merah, Singapore 169547.
[3] To whom correspondence should be addressed. Tel.: 801-581-4967; Fax: 801-581-6001; E-mail: diane.mcveyward@path.utah.edu.
[4] The abbreviations used are: YMon1, yeast Mon1; BFA, brefeldin A; DHC1, dynein-heavy chain; Endo H, endoglycosidase H; ER, endoplasmic reticulum; ERES, ER exit sites; ERGIC, ER-Golgi intermediate compartment; GalNAc-T2-GFP, Golgi protein *N*-acetylgalactosaminyltransferase-2-green fluorescent protein; PNS, postnuclear supernatant; VSVG-GFP, vesicular stomatitis virus G protein-GFP; DIC, dynein intermediate chain; COPII, coat complex II.

Jolla, CA) or pEGFPC1 (Clontech). YFP-ER and YFP-Golgi were obtained from Clontech. All constructs were sequence verified prior to use.

Treatment with siRNA Oligonucleotide Pools—Cells were treated with nonspecific, Mon1a-specific, or dynein heavy chain 1-specific oligonucleotides (Dharmacon SiGenome SiRNA SMARTpool) (Dharmacon RNA Technologies, Lafayette, CO) using Oligofectamine reagent (Invitrogen) according to the manufacturer's instructions.

Yeast Strains and Growth Media—Wild type (BY4743), Δ*mon1*, and Δ*ccz1* strains were obtained from the Research Genetics (Invitrogen) homozygous diploid deletion collection. Cells were transformed with pYES2.0 (Invitrogen), pYES2.0mouseMon1a-FLAG, or pYES2.0mouseMon1b-FLAG for GAL1-regulated expression, with pMET3humanc7orf28b-myc for MET3-regulated expression, or with pRS426FLAG-MON1 or pRS416FLAG-MON1. The yeast promoter was defined as 1,000 bp upstream of the *MON1* open reading frame. Yeast strains were grown in YPD medium (1% yeast extract, 2% peptone, 2% dextrose) or in complete minimal medium (0.67% yeast nitrogen base without amino acids, 2% dextrose or galactose, and 0.13% amino acid drop-out mix). Complete minimal medium was supplemented with 5 mM $ZnCl_2$, and cells were grown for 2–4 days at 30 °C.

FM4-64 Vacuole Staining—Yeast strains were grown overnight to log phase. 10 optical densities of yeast were pelleted and resuspended in 1.0 ml of growth medium. Cell were given 5.0 μM FM4-64 diluted according to the manufacturer's instructions (Invitrogen), and cells were incubated for 10 min at 30 °C. Cells were washed and placed back in growth media lacking FM4-64 for 45 min at 30 °C. 10 μl of cells were spotted onto concanavalin A-coated coverslips, and vacuole morphology was examined by epifluorescence and Nomarski microscopy. Images were captured using an Olympus BX51 upright microscope with a 100× 1.4NA objective and the Optronics PictureFrame software (Olympus Inc., Melville, NY).

Subcellular Fractionation—NIH3T3 cells were grown on 100-mm tissue culture plates. For crude subcellular fractionation, cells were scraped into phosphate-buffered saline (PBS), pelleted at 1,000 × *g* for 5 min, and resuspended in 2.0 ml of 0.25 M sucrose, 10 mM Tris-HCl, pH 7.2, 0.5 mM EDTA. Cells were homogenized with a ball-bearing homogenizer and centrifuged at 800 × *g* for 5 min, and a postnuclear supernatant (PNS) was obtained. The PNS was centrifuged at either 6,552 × *g* (10,000 rpm) for 20 min or 191,056 × *g* (54,000 rpm) for 40 min to obtain membrane and cytosolic fractions. For further subcellular fractionation, the PNS was overlaid onto a 23% Percoll (GE Healthcare) gradient and centrifuged at 54,000 rpm for 30 min, and gradients were fractionated bottom to top. Fractions of the gradient were analyzed for organellar markers using SDS-PAGE followed by Western blot. The samples were solubilized in 1.0% Triton X-100, and protein determinations were performed to normalize for protein using the bicinchoninic acid assay (Pierce) and 25 or 50 μg of protein/sample loaded onto SDS-PAGE gels.

Brefeldin A Treatment—Cells plated on glass coverslips were incubated with 5 μg/ml brefeldin A (BFA) (Epicenter Biotechnologies, Madison, WI) for 30 min, washed three times, and placed in growth medium for recovery. Wild type VSVG-GFP and ts045VSVG-GFP were expressed in NIH3T3 cells that were maintained at either 32 °C or the restrictive temperature (39 °C) followed by shifting to the permissive temperature (32 °C). VSVG-GFP was considered ER-associated if VSVG-GFP could be visualized within ER compartments (nuclear ring, reticulum), whereas VSVG-GFP was considered Golgi-associated once VSVG-GFP was deposited within Golgi (perinuclear and "stacked") and plasma membrane once VSVG-GFP could be visualized as a concentrated line at the cell edge as described previously (10). GalNAc-T2-GFP HeLa cells were BFA-treated and recovered at 37 °C. BFA recovery was visualized using an Olympus BX51 upright microscope with a 100× 1.4NA objective and the Optronics PictureFrame software (Olympus).

ts045VSVG-GFP Trafficking and [^{35}S]Methionine Metabolic Labeling—Cells silenced with nonspecific, Mon1a, or DHC1 oligonucleotides were transfected with ts045VSVG-GFP and maintained at the restrictive temperature (39 °C). Cells were moved to the permissive temperature (32 °C), and movement of ts045VSVG-GFP to the plasma membrane over time was assessed by fluorescent microscopy. The data are expressed as the percentage of cells showing VSVG-GFP at the plasma membrane. For metabolic labeling, cells maintained at 39 °C were grown in DMEM-methionine for 2 h. Cells were pulsed with [^{35}S]methionine (PerkinElmer Life Sciences) for 20 min, washed, shifted to 32 °C for various times in the presence of DMEM with excess methionine, lysed in 1.0% Triton X-100, 150 mM NaCl, 0.5 mM EDTA (lysis buffer), and immunoprecipitated with rabbit anti-GFP (Abcam, Cambridge, MA) and protein A/G-agarose (Santa Cruz Biotechnology, Santa Cruz, CA). Following immunoprecipitation, samples were denatured and incubated with or without endoglycosidase H (New England Biolabs, Ipswich, MA) for 2 h, samples were heated to 100 °C for 10 min and separated on SDS-PAGE, and ^{35}S-labeled VSVG-GFP was detected by autoradiography.

Transfections and Western Analysis—HeLa cells, bone marrow-derived macrophages, and NIH3T3 fibroblasts were plated onto tissue culture plates and allowed to grow for 24–48 h to 50–80% confluence. The cells were transfected with various constructs using Amaxa nucleofector technology (Lonza, Walkersville, MD) according to the manufacturer's directions. Protein expression was determined by solubilizing 2–4 × 10^6 cells in lysis buffer plus 2× protease inhibitor mixture (Roche Applied Science) and 1.0 mM phenylmethylsulfonyl fluoride (Sigma-Aldrich). Samples were analyzed by SDS-PAGE, and Western analysis was performed using mouse anti-FLAG antibody (1:1000; Sigma-Aldrich); rabbit anti-GFP (1:5000, ab6556; Abcam); mouse anti-tubulin (1:1000; GeneTex, San Antonio, TX); mouse anti-p115 (1:500, GeneTex); rabbit anti-ERGIC-53 (1:1000, Sigma-Aldrich); mouse anti-DIC (1:2000, MMS-400R Covance, Princeton, NJ); or DHC1 (1:1000, Abcam) followed by either peroxidase-conjugated goat anti-mouse immunoglobulin IgG (1:5,000; Jackson ImmunoResearch Laboratories, West Grove, PA) or peroxidase-conjugated goat anti-rabbit IgG (1:5,000; Jackson ImmunoResearch Laboratories). Antibodies to Mon1a were generated as described (9). Rabbit anti-Mon1a was used at a concentration of 1:500 followed by peroxidase-conjugated

goat anti-rabbit IgG (1:5,000) (Jackson ImmunoResearch Laboratories). The blots were developed using Western Lightning reagent (PerkinElmer Life Sciences). Tubulin was used as a loading control. All experiments were performed a minimum of three times, and error bars represent S.E.

Epifluorescence, Immunofluorescence, and Electron Microscopy—Cells were incubated with 20 μg/ml Texas Red dextran overnight at 37 °C, washed, and chased for 2 h to move all dextran to lysosomes as described previously (11) (12). Cells were incubated with 5 μg/ml Alexa Fluor 488-Tf(Fe)$_2$ for 30 min to load the early endocytic pathway as described previously (13, 14). Live cell images were captured on a confocal microscope or an epifluorescence microscope. Vesicle size was determined manually by measuring the area of the vesicles as described previously using the ImageJ software (15). For immunofluorescence, cells were fixed in 3.7% formaldehyde/PBS, permeabilized in 0.1% saponin/PBS/BSA, and incubated with mouse anti-Sec31 (1:100; BD Biosciences), rabbit anti-Giantin (1:100; Covance), rabbit anti-ERGIC-53 (1:100; Sigma), rabbit anti-GFP (1:500; GeneTex), or mouse anti-p115 (1:500, GeneTex) followed by Alexa Fluor 594-, Alexa Fluor 647-, or Alexa Fluor 488-conjugated goat anti-rabbit or anti-mouse IgG (1:750, Invitrogen). Confocal images were captured on an Olympus FV1000 microscope with a 60× 1.4NA oil immersion objective. Image analysis and quantification were performed using the Volocity software. For electron microscopy (EM), cells were fixed in 2.5% glutaraldehyde, 1% paraformaldehyde, and transmission EM images were captured at the University of Utah EM Core.

Immunoprecipitation—Cells were transfected with pFLAG-Mon1a or GFP-Mon1a, solubilized in lysis buffer, incubated at 0 °C for 30 min, centrifuged at 10,000 × *g*, 10 min, and immunoprecipitated using mouse anti-FLAG antibody (Sigma) or rabbit anti-GFP (GeneTex) and protein A/G-agarose (Santa Cruz Biotechnology). Proteins in the immunoprecipitate were identified using Western blot analysis as described above, and mass spectrometry was performed at the University of Utah Mass Spectrometry Core as described previously (16).

RESULTS

Overexpression of Mammalian Mon1a or Mon1b in Yeast Does Not Suppress the Phenotypes Associated with Loss of MON1 or CCZ1—Studies of Mon1 in *S. cerevisiae* have suggested that Mon1 is involved in vacuole fusion (1–3). More recently, Mon1 and its partner Ccz1 have been shown to act as a guanine nucleotide exchange factor of the late endosomal rab7 homolog Ypt7 in *S. cerevisiae* (17). Mammals have two Mon1 genes, Mon1a and Mon1b. Previously, we determined that reductions in Mon1a did not affect endocytosis or phagocytosis (9). We further determined that reductions in Mon1a did not affect the morphology of lysosomes or early and recycling endosomes (supplemental Fig. 1). To determine whether mammalian Mon1a or Mon1b could complement the loss of Mon1 in *S. cerevisiae*, we generated yeast plasmids containing epitope-tagged mammalian Mon1a or Mon1b under the regulation of the *GAL1* promoter. We determined that Mon1a and Mon1b did not complement the loss of *MON1* or *CCZ1* in *S. cerevisiae* based upon vacuole morphology, growth on $ZnCl_2$-containing medium, and carboxypeptidase Y secretion (supplemental Fig. 2). Similarly, expression of the Mon1a or Mon1b along with the putative mammalian homologue of the Mon1 yeast partner protein Ccz1, human c7orf28b, did not complement the loss of *MON1* or *CCZ1* in *S. cerevisiae*, although the proteins were expressed (data not shown). We also note that c7orf28b did not complement the loss of *CCZ1* (data not shown). These results suggest either that the mammalian homologue cannot interact with the machinery in yeast needed for function or that the mammalian homologues have evolved to perform different functions.

siRNA-mediated Reductions of Mon1a Result in Delayed Secretion—Our previous studies suggest that Mon1a may have a role in the secretory pathway (9). To determine where Mon1a acts in the secretory pathway, we treated NIH3T3 cells with the fungal metabolite BFA, an inhibitor of the GTP exchange factor for ADP-ribosylation factor 1, which ultimately inhibits protein transport from ER to Golgi, redistributing the Golgi apparatus into the ER. Removal of BFA allows recovery of anterograde movement, and proteins will resume trafficking to reassemble the Golgi apparatus. We utilized Mon1a-specific siRNA oligonucleotide pools to reduce the levels of Mon1a in NIH3T3 cells transfected with a plasmid containing vesicular stomatitis virus G protein with a green fluorescent protein tag (VSVG-GFP). We treated cells with BFA and examined the effects of Mon1a reduction on the rate of movement of VSVG-GFP during BFA recovery. Mon1a levels were efficiently reduced in NIH3T3 cells (Fig. 1*A*). BFA treatment resulted in VSVG-GFP condensing down into a perinuclear ER structure as expected. Reductions in Mon1a did not affect the collapse of the Golgi apparatus in response to BFA. In nonspecifically silenced cells, 60% of cells had VSVG-GFP on the plasma membrane within 45 min of removal of BFA (Fig. 1*B*). In contrast, at the same time, less than 20% of Mon1a-silenced cells showed VSVG-GFP on the plasma membrane.

To ensure that the observations made with BFA treatment were not the result of global effects of BFA on all membrane trafficking, we utilized a temperature-sensitive allele of VSVG termed ts045VSVG-GFP that is localized to the ER at the restrictive temperature (39 °C) but moves through the Golgi apparatus to the plasma membrane at the permissive temperature (32 °C) (18). Cells treated with nonspecific or mouse Mon1a-specific siRNA were transfected with ts045VSVG-GFP, grown at the restrictive temperature for 18 h, and then moved to the permissive temperature to assess ts045VSVG-GFP trafficking. Again, reduction of Mon1a levels delayed the movement of ts045VSVG-GFP from ER to plasma membrane (Fig. 1*C*) when compared with control cells, confirming that the effects seen with BFA treatment were specific to Mon1a knockdown.

Reductions in Mon1a Affect Golgi Apparatus Morphology and Trafficking—To determine whether reductions in Mon1a affected the trafficking of ts045VSVG-GFP from Golgi to plasma membrane, we placed cells at 15 °C to allow the ts045VSVG-GFP to accumulate in the Golgi and then shifted cells to 24 °C to slow the rate of movement of ts045VSVG-GFP from Golgi to plasma membrane (19). Reductions in Mon1a delayed the movement of ts045VSVG-GFP from the Golgi to

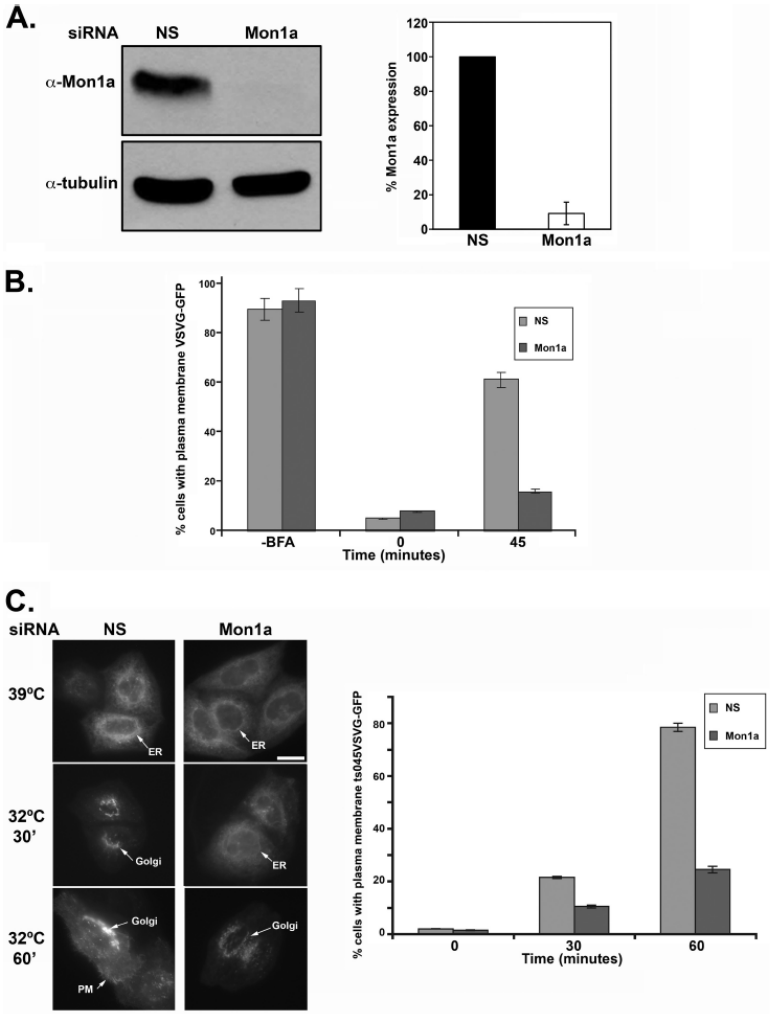

FIGURE 1. **Trafficking of VSVG-GFP is delayed in Mon1a-silenced cells.** *A*, NIH3T3 cells expressing VSVG-GFP were silenced with nonspecific (*NS*) or Mon1a specific oligonucleotide pools for 48–72 h. Cells were lysed, and the levels of Mon1a and tubulin were assessed by Western blot. A representative blot is shown with the graph representing the average knockdown from $n = 3$ blots. *Error bars* represent the S.E. *B*, cells as in *A* were treated with 5 μg/ml BFA for 30 min at 37 °C, BFA was removed, cells were placed in DMEM at 37 °C, and VSVG-GFP trafficking to the plasma membrane was assessed by epifluorescence microscopy. The data are expressed as the percentage of cells showing VSVG-GFP localization at the plasma membrane −BFA, +BFA (time 0), and 45 minutes, examining localization with 50–100 cells per sample counted. *Error bars* represent the S.E. *C*, cells silenced for Mon1a were transfected with ts045VSVG-GFP and maintained at the restrictive temperature (39 °C). Cells were moved to the permissive temperature (32 °C), and movement of ts045VSVG-GFP to the plasma membrane over time was assessed by fluorescent microscopy. Representative images at 39 °C, 32 °C 30 min and 32 °C 60 min are shown. *Scale bar* = 10 μm. *Arrows* denote reticular ER, Golgi, or plasma membrane (*PM*). Images were analyzed and quantified by three separate individuals. The data are expressed as the percentage of cells showing ts045VSVG-GFP at the plasma membrane as described under 'Experimental Procedures.' All experiments were performed a minimum of five times. *Error bars* represent the S.E.

the cell surface when compared with control cells (Fig. 2*A*). Reductions in Mon1a altered the morphology of the Golgi apparatus as assessed by electron microscopy (Fig. 2*B*) and immunofluorescence (Fig. 2*C*). Golgi-like compartments were visible in Mon1a-silenced cells; however, the tight organization or stacking of the Golgi apparatus seen in nonspecifically silenced cells was lost. Rather, Mon1a-silenced cells showed more extended, unstacked Golgi morphology.

Mon1a Regulates Early and Late Trafficking in the Secretory Pathway—The above experiments show that loss of Mon1a affects trafficking through the secretory pathway and Golgi morphology. We focused our attention on how Mon1a affects ER-to-Golgi trafficking. Mon1a was silenced in a HeLa cell line stably expressing a GFP fusion of the resident Golgi enzyme *N*-acetylgalactosaminyltransferase-2 (GalNAc-T2). This marker can be used along with BFA treatment to assess the

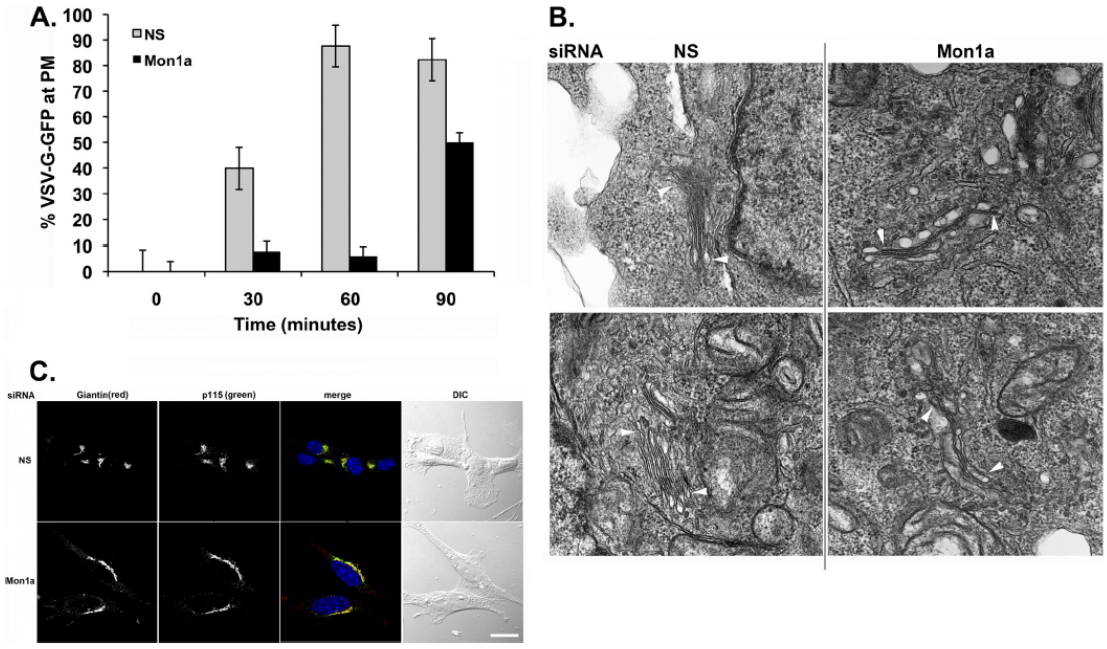

FIGURE 2. **Reductions in Mon1a alter Golgi morphology.** *A*, cells as in Fig. 1*C* were shifted from 39 to 15 °C to allow all ts045VSVG-GFP to accumulate in the Golgi (4–8 h). Cells were then shifted to 24 °C to allow movement of ts045VSVG-GFP to the plasma membrane (*PM*), and images were captured over time. The data are expressed as the percentage at the plasma membrane. All experiments were performed a minimum of three times. *Error bars* represent the S.E. *NS*, nonspecific. *B*, cells silenced as in *A* were processed for EM as described under 'Experimental Procedures.' Magnification = 70,000×. *Arrowheads* identify Golgi structures in nonspecifically (*NS*) or Mon1a-silenced cells. *C*, mouse fibroblasts were silenced with nonspecific or mouse Mon1a-specific oligonucleotides for 96 h, fixed, and processed for immunofluorescence using rabbit anti-Giantin or mouse anti-p115. Images were captured on an Olympus FV1000 confocal microscope. Representative images are shown from $n = 3$ separate experiments. *Scale bar* = 10 μm. *Arrows* denote altered Golgi structures in Mon1a-silenced cells.

kinetics of Golgi reassembly, which requires functional anterograde transport (20). In the presence of BFA, GalNAc-T2 is redistributed to the ER (Fig. 3*A*). Complete recovery of the Golgi complex after BFA removal was observed at 2–3 h in control cells, as described previously (20). In contrast, Golgi localization of GalNAc-T2 following BFA treatment was delayed in Mon1a-silenced cells (6–8 h). Expression of an siRNA-resistant FLAG-tagged murine Mon1a allele in HeLa cells silenced for Mon1a restored Golgi recovery, after BFA treatment, back to control. These results demonstrate that the amino terminally FLAG-tagged mouse Mon1a is functional and complemented the loss of human Mon1a and that impaired ER-to-Golgi traffic was a specific effect of Mon1a reduction as opposed to an off-target effect of RNAi.

To examine whether reduction of Mon1a protein levels affects ER-to-Golgi traffic independent of the use of BFA, we utilized a well characterized endoglycosidase H (Endo H) sensitivity assay. Membrane proteins in the ER are *N*-linked glycosylated, resulting in a high mannose-containing carbohydrate, which is a substrate for endoglycosidase H (for review, see Ref. 21). Once membrane proteins move to the *medial*-Golgi, the carbohydrate moieties are modified, and *N*-linked glycosylated proteins become resistant to Endo H. ts045VSVG-GFP is glycosylated in this manner and is sensitive to Endo H when cells are maintained at the restrictive temperature (ER) and becomes resistant when cells are moved to the permissive temperature (Golgi). We took advantage of ts045VSVG-GFP and the Endo H sensitivity of ER-localized glycoproteins to determine whether Mon1a acts in early secretory membrane trafficking. siRNA-treated cells expressing ts045VSVG-GFP were kept at the restrictive temperature. Cells treated with nonspecific or Mon1a-specific oligonucleotide pools showed Endo H-sensitive ts045VSVG-GFP at the nonpermissive temperature (Fig. 3*B*). Endo H sensitivity of ts045VSVG-GFP was lost in nonspecifically silenced cells as early as 10 min after shifting to the permissive temperature. In contrast, cells silenced for Mon1a showed a significant delay in ts045VSVG-GFP gaining Endo H resistance. These data support the hypothesis that Mon1a functions in ER-to-Golgi trafficking.

Mon1a Is a Cytosolic Protein That Peripherally Associates with the ER—We previously demonstrated that Mon1a is ubiquitously expressed in all tissues of mice and is predicted to be a 68-kDa cytosolic protein (9). To determine the localization of Mon1a, we homogenized mouse NIH3T3 fibroblasts and separated the membrane and cytosolic fractions. A large percentage of endogenous Mon1a was associated with the membrane fraction (Fig. 4*A*). Treatment of the membrane fraction with Na_2CO_3, a procedure that disrupts ionic interactions, showed that Mon1a is not an integral membrane protein but rather is a peripheral membrane protein that associates with the mem-

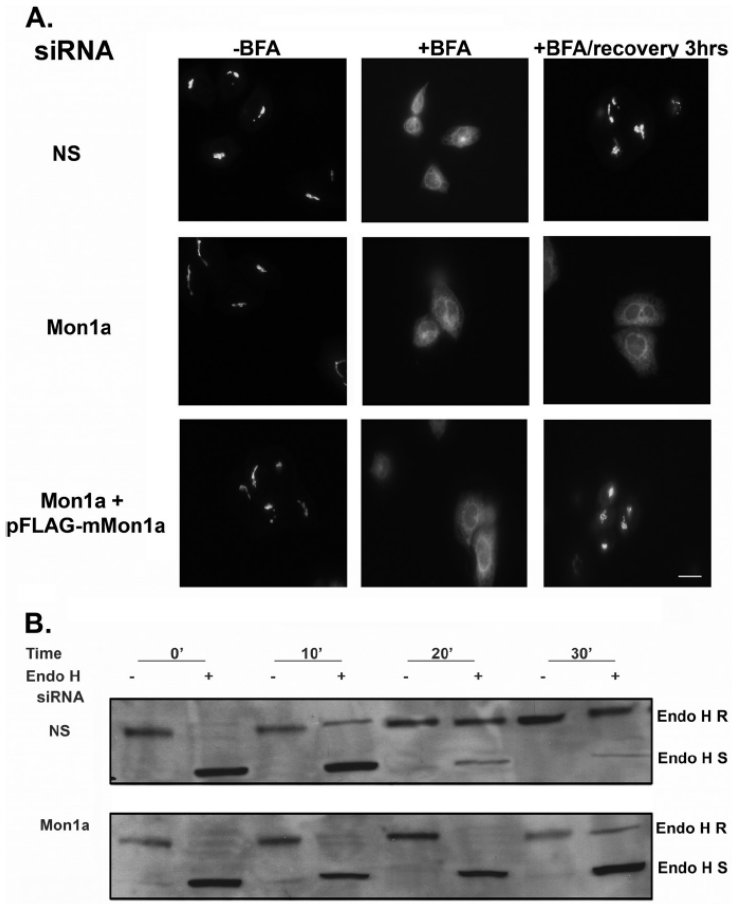

FIGURE 3. **Reductions in Mon1a affect trafficking from the ER to the Golgi.** *A*, HeLa cells stably expressing GalNAc-T2-GFP were silenced with nonspecific (*NS*) or human Mon1a specific oligonucleotides for 72 h. Cells were than transfected with empty vector or siRNA-resistant mouse FLAG-Mon1a and incubated for 18 h. Cells were then treated with BFA as in Fig. 1, BFA was washed away, and the movement of GalNAc-T2-GFP to the Golgi apparatus was assessed by epifluorescence microscopy. Representative images are shown from $n = 5$ experiments. *Scale bar* = 10 μm. *B*, NIH3T3 cells nonspecifically or Mon1a-silenced expressing ts045VSVG-GFP were grown in methionine-depleted DMEM for 2 h at 39.5 °C. Cells were then pulsed with [^{35}S]methionine for 30 min at 39.5 °C and shifted to 32 °C for the indicated times. Cells were lysed in 1% Triton X-100, 0.15 M NaCl, 10 mM Tris-HCl, pH 7.2. Lysates were immunoprecipitated for GFP, denatured, and incubated with Endo H for 2 h, and radiolabeled ts045VSVG-GFP was resolved on SDS-PAGE followed by autoradiography. A representative blot ($n = 3$) is presented. *R*, Endo H resistant; *S*, Endo H sensitive.

brane in a noncovalent interaction (Fig. 4*B*). The Mon1a polyclonal antibody used for Western analysis was not effective for immunofluorescence; therefore, we epitope-tagged Mon1a with GFP, confirmed that it was functional similar to FLAG-tagged Mon1a (data not shown), and examined localization by epifluorescence microscopy. GFP-Mon1a was found primarily in the cytosol with some reticular membrane localization (Fig. 4*C*). One caveat to these results is that GFP-Mon1a is highly overexpressed and may not reflect endogenous localization. We performed subcellular fractionation on cells expressing FLAG-Mon1a and either an ER-localized yellow fluorescent protein (YFP-ER) or a Golgi-localized YFP (YFP-Golgi). Endogenous and FLAG-tagged Mon1a were found primarily coincident with YFP-ER and to a lesser degree with YFP-Golgi (Fig. 4*D*). These results suggest that Mon1a associates with early secretory pathway membranes.

Mon1a Interacts with the Microtubule-based Molecular Motor Dynein—To determine how Mon1a functions in the early secretory pathway, we utilized our epitope-tagged Mon1a (FLAG-Mon1a) to immunoprecipitate Mon1a and examined the immunoprecipitate for possible partners by mass spectrometry. Immunoprecipitated Mon1a (Fig. 5*A*) was subsequently analyzed by LC/MS/MS, and dynein intermediate chain (DIC) was found associated with Mon1a. We confirmed that DIC coimmunoprecipitated with FLAG-Mon1a using Western blot analysis. This interaction was specific as another FLAG-tagged protein, Lip5, which is involved in multivesicular body formation (16), did not coimmunoprecipitate DIC. Dynein is a mul-

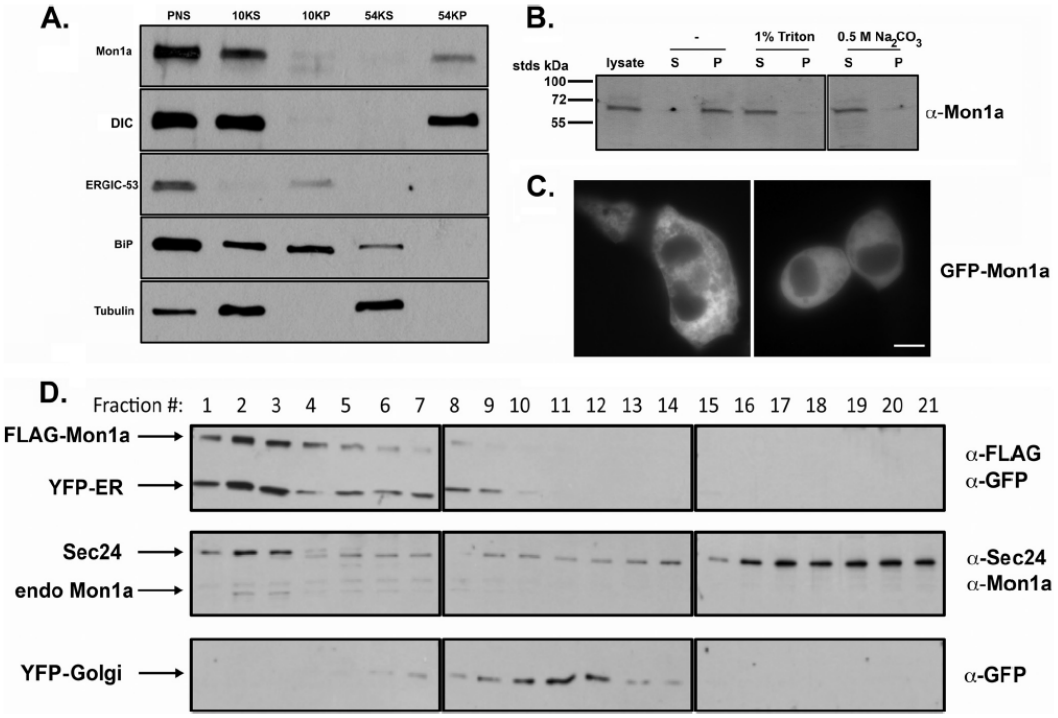

FIGURE 4. **Mon1a is a cytosolic protein that peripherally associates with the ER.** *A*, NIH3T3 cells were homogenized in 0.25 M sucrose, 10 mM Tris-HCl, 0.5 mM EDTA and centrifuged at 800 × *g* for 5 min, and PNS was obtained and centrifuged at 6,552 × *g* (*10KP*). Supernatant from the 10,000 spin (*10KS*) was then centrifuged at 191,056 × *g* for 30 min (*54KS* and *54KP*). Membrane and cytosolic fractions were solubilized in SDS-PAGE sample buffer, and the presence of Mon1a, DIC, ERGIC-53, BiP, and tubulin was determined by Western blot. *B*, membranes as in *A* were treated with 1% Triton X-100 or 0.5 M Na_2CO_3 and repelleted prior to SDS-PAGE, and Western blot analysis for endogenous Mon1a was performed. *S*, supernatant; *P*, pellet. *C*, cells were transfected with pGFP-Mon1a. 24 h after transfection, GFP-Mon1a localization was assessed by epifluorescence microscopy. Two representative images are shown. *D*, NIH3T3 cells expressing either a YFP-ER or a YFP-Golgi marker and FLAG-Mon1a were homogenized as in *A*. The postnuclear supernatants (800 × *g*) from YFP-ER/FLAG-Mon1a or YFP-Golgi/FLAG-Mon1a were top-loaded onto a 23% Percoll gradient, centrifuged at 54,000 × *g* for 30 min, and fractionated, and the presence of YFP-ER or YFP-Golgi and endogenous Mon1a, Sec24, and FLAG-Mon1a was examined by Western blot analysis. Endogenous Mon1a, Sec24, and FLAG-Mon1a from YFP-ER samples are shown along with YFP-Golgi from a separate gradient to show Golgi localization. All experiments were performed a minimum of three times.

tisubunit motor protein involved in many vesicle trafficking events, and its function in the secretory pathway is well documented (22–24). Dynein attaches to membranes often through the intermediate chain and to microtubules through the heavy chain to move vesicles on microtubule tracks, and a role for dynein in vesicle formation from the ER has been suggested (23, 24). We silenced DHC1 and noted that loss of DHC1 resulted in a concomitant loss of DIC (Fig. 5*B*). Cells silenced for DHC1 showed a fragmented Golgi morphology (Fig. 5*C*, −BFA and supplemental Fig. 3*A*). Reductions in both Mon1a and DHC1 showed a reduced fragmentation of the Golgi when compared with DHC1 alone, suggesting that Mon1a is needed for the Golgi fragmentation seen in DHC1-silenced cells.

Previous studies have shown that the dynein-dynactin complexes are important in coordinating microtubule-mediated exit from the ER (23). Those studies showed that ER exit is mediated through dynactin directly interacting with Sec23, a COPII coat protein necessary for vesicle budding off the ER (25). BFA treatment of DHC1-silenced cells showed delayed reformation of the Golgi apparatus similar to reductions in Mon1a (Fig. 5*C*). Reductions in DHC1 also resulted in a delay in ts045VSVG-GFP gaining Endo H resistance (supplemental Fig. 3*B*), confirming that dynein is important in anterograde trafficking between the ER and the Golgi.

Confocal microscopic analysis of the Golgi after Mon1a and DHC1 silencing was performed using the GalNAc-T2-GFP HeLa cells. The Volocity software was used to quantify the alterations in Golgi morphology observed in Mon1a and DHC1-silenced cells. There were significant changes in the average surface area and the average volume of the Golgi apparatus in Mon1a- or DHC1-silenced cells, demonstrating a role for both proteins in maintaining Golgi morphology (Fig. 6). DHC1-silenced cells also showed an increased number of Golgi elements indicative of fragmentation. Silencing of Mon1a in DHC1-silenced cells reduced the amount of fragmentation seen with loss of DHC1 alone; however, the number of elements still remained higher than in cells that were treated with nonspecific oligonucleotides. The average surface area and volume of the Golgi elements remained similar to silencing DHC1. This quantification suggests that the high level of Golgi fragmentation seen in DHC1-silenced cells is affected by the levels of Mon1a.

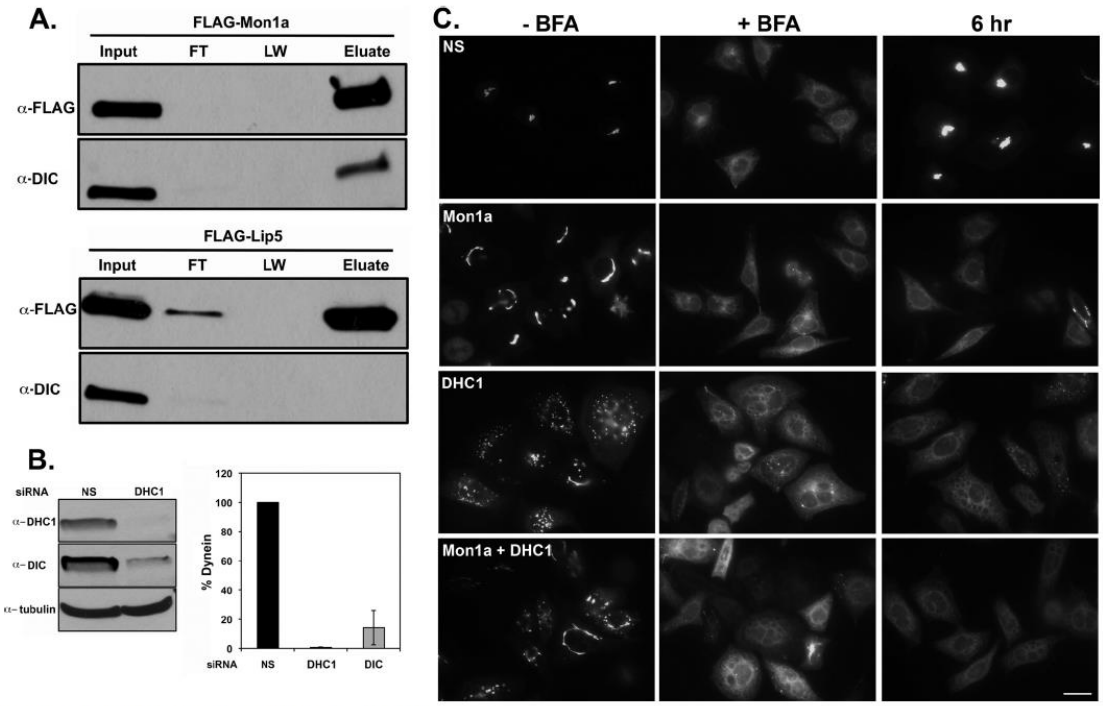

FIGURE 5. **FLAG-Mon1a interacts with dynein, and reductions in DHC1 delay trafficking from ER to Golgi.** *A*, NIH3T3 cells were transfected with pFLAG-Mon1a or pFLAG-Lip5 (as a negative control). 24 h after transfection, cells were harvested, incubated in lysis buffer at 0 °C for 30 min, and centrifuged for 30 min at 22,000 × *g*, and the supernatant was incubated with mouse anti-FLAG antibody and protein A/G beads for 18 h at 4 °C. Beads were washed and eluted in 2× sample buffer at 100 °C for 10 min, proteins in the lysate (*Input*), flow-through (*FT*), and last wash of three (*LW*) and eluate were examined for FLAG-Mon1a by Western blot, and mass spectrometry was performed on these samples (data not shown). FLAG-Mon1a immunoprecipitates were probed for DIC. All experiments were performed a minimum of three times. *B*, NIH3T3 cells were silenced with nonspecific (*NS*) or DHC1 specific oligonucleotide pools for 72–96 h. Cells were lysed, and the levels of DHC1, DIC, and tubulin were assessed by Western blot. A representative blot is shown. Blots were quantified using tubulin as a loading control $n = 3$. *C*, HeLa cells stably expressing GalNAc-T2-GFP were silenced with nonspecific, Mon1a, and/or human DHC1 specific oligonucleotides for 72 h. Cells were then treated with BFA as in Fig. 1, BFA was washed away, and the movement of GalNAc-T2-GFP to the Golgi apparatus was assessed by epifluorescence microscopy. Representative images for −BFA and +BFA and at 6 h of recovery are shown from $n = 5$ experiments. *Scale bar* = 10 μm.

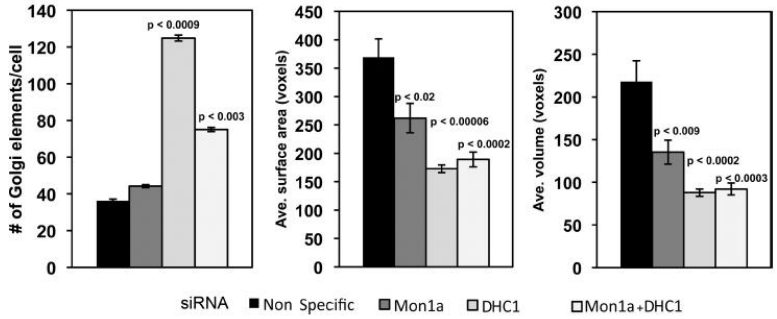

FIGURE 6. **Volocity analysis and quantification of changes in Golgi morphology in Mon1a, dynein heavy chain, or Mon1a + dynein heavy chain silenced cells.** Cells silenced as in Fig. 5 were imaged using confocal microscopy, and images were quantified using the Volocity software. The Golgi-labeled channel was quantified by setting the lower size cutoff limit at 10 cubic voxels, which is just above the minimum optically resolvable volume to filter out digital noise. Cells were cropped out of the image and measured individually to get cell-by-cell data. Signal was thresholded using the same intensity values for all silenced groups. The data are expressed as the number of Golgi elements/cell, and the average (*Ave.*) Golgi surface area and average Golgi volume are expressed as voxels (cubic pixel area). All experiments were performed a minimum of three times. *Error bars* represent the S.E. *p* values were determined using a two-tailed Student's *t* test statistical analysis comparing them with the nonspecifically silenced cells.

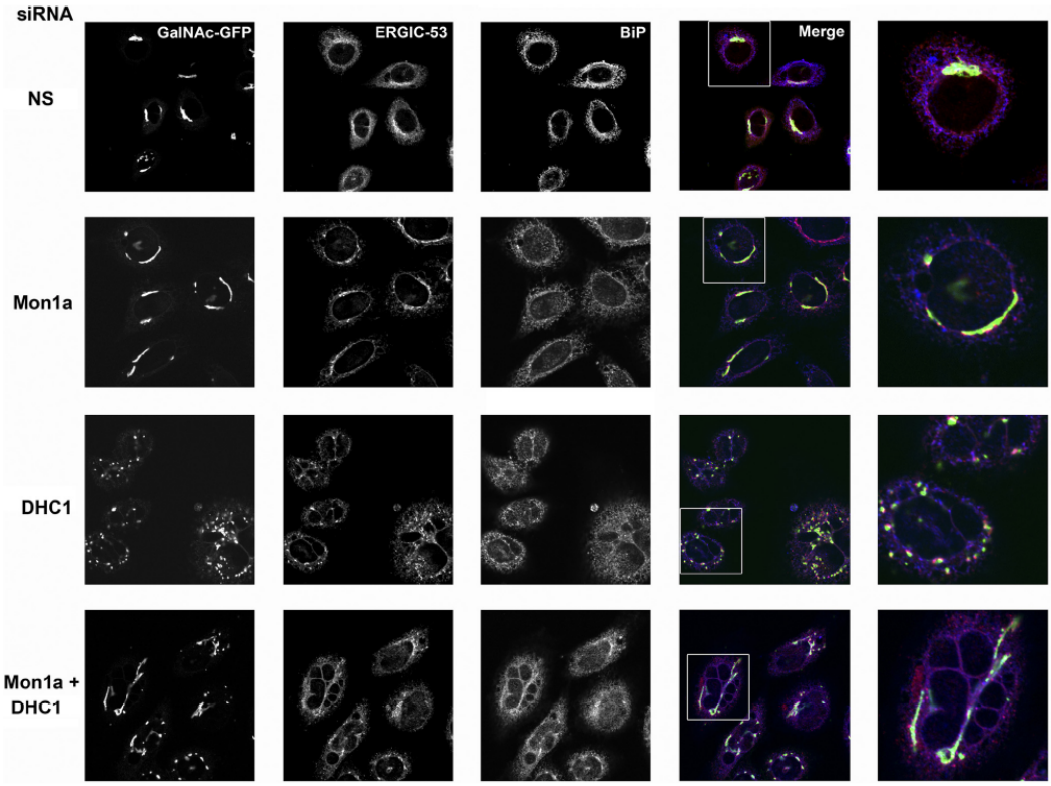

FIGURE 7. **Reductions in Mon1a or DHC1 affect steady state Golgi and ERGIC-53 morphology.** HeLa cells expressing GalNAc-T2-GFP (*green*) incubated with nonspecific (*NS*), Mon1a, or DHC1 oligonucleotides. 72 h after siRNA, cells were fixed, permeabilized, and incubated with mouse anti-ERGIC-53 (*red*) and rabbit anti-BiP (pseudocolored *blue*) followed by Alexa Fluor 594-conjugated goat anti-mouse and Alexa Fluor 647-conjugated goat anti-rabbit and imaged using a 60× oil immersion objective and an Olympus FV1000 confocal microscopy. *Z* stacks were captured every 0.5 μm, and a single plane projection showing coincidence is shown ($n = 3$). Images are representative fields with the *far right panel* a zoom of the *boxed area*. *Scale bar* = 10 μm.

Reductions in Mon1a Delay the Formation of ER-derived Vesicles—ER exit sites (ERES) and vesicle formation require the recruitment of COPII onto ER exit sites (for review, see Zanetti *et al.* (31)). To determine whether COPII recruitment was affected by reductions in Mon1a or DHC1, we examined the localization of the COPII protein Sec31 in Mon1a- or DHC1-silenced cells during BFA recovery. Sec31, a component of the outer COPII coat, was recruited to ER exit sites in the presence or absence of Mon1a or DHC1 (supplemental Fig. 4). We note that Sec31 showed a high degree of coincidence with the Golgi marker GalNAc-T2-GFP as reported previously (26); however, the localization was not different in the presence or absence of Mon1a or DHC1. DHC1 silencing frequently resulted in an increased number of nuclei per cell. We also note that there appeared to be increased numbers of Sec31-positive sites present in Mon1a- or DHC1-silenced cells, possibly as a consequence of delayed reformation of the Golgi apparatus. These data demonstrate that Mon1a and DHC1 are not necessary for COPII recruitment and that they function after coat assembly.

Once COPII proteins are recruited to ERES, then the newly formed vesicles can acquire the mannose-specific membrane lectin ERGIC-53, which acts as a receptor for glycoprotein trafficking to the ERGIC or vesicular-tubular compartment between the ER and Golgi (27). It is possible that reductions in Mon1a or DHC1 affect the ability to recruit ERGIC-53, and subsequently, GalNAc-T2-GFP would not be trafficked in the reformation of the Golgi apparatus. We examined the localization of ERGIC-53 in Mon1a- and DHC1-silenced GalNAc-T2-GFP cells using confocal microscopy. Mon1a-silenced cells showed an increased perinuclear localization of ERGIC-53 surrounding the nucleus when compared with nonspecifically silenced cells (Fig. 7). DHC1-silenced cells also showed increased perinuclear ERGIC-53 localization similar to Mon1a-silenced cells. We note that the resident ER protein BiP appeared unchanged, suggesting that reductions in Mon1a or DHC1 do not significantly affect ER morphology.

The loss of Mon1a or dynein could affect the budding of vesicles from the ER or the fusion of budded vesicles with the ERGIC or Golgi. To determine whether the loss of Mon1a or DHC1 and concomitantly DIC affects the formation of ER-derived vesicles, we followed the movement of ERGIC-53 into ER-derived vesicles. Microsomal membranes can be pelleted at low speeds, whereas ER-derived vesicles require higher speed centrifugation (28). Nonspecifically silenced, Mon1a-silenced,

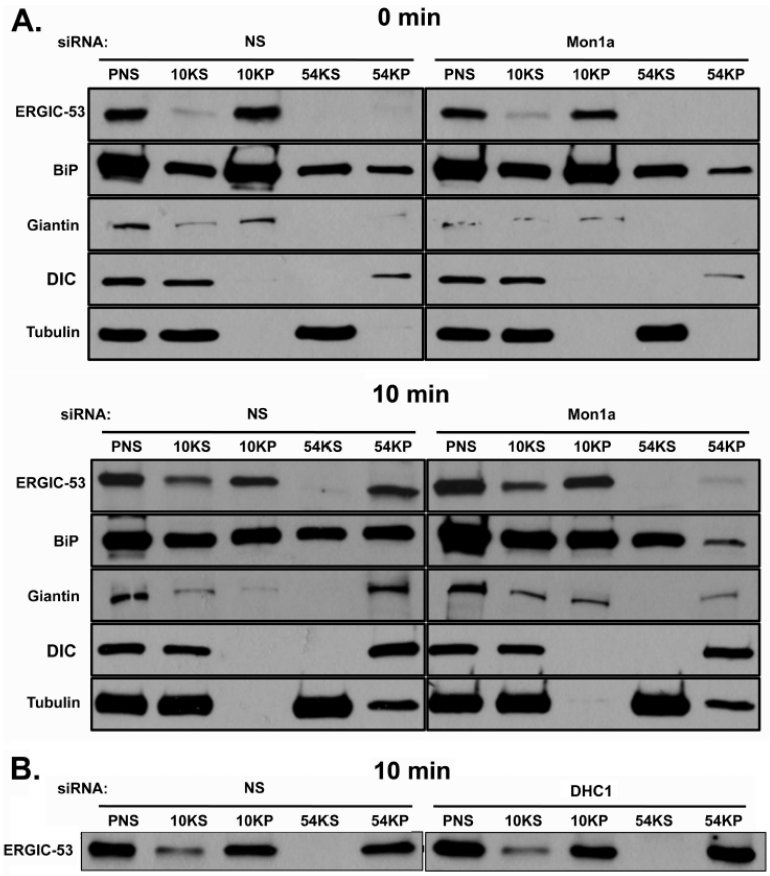

FIGURE 8. **Silencing of Mon1a delays formation of ERGIC-53-positive vesicles off the ER.** *A*, NIH3T3 cells nonspecifically (*NS*) or Mon1a-silenced were treated with BFA as in Fig. 1. BFA was removed, cells were incubated for 10 min at 37 °C and homogenized, homogenates were centrifuged at 800 × *g* for 5 min (PNS), supernatant was centrifuged at 6,552 × *g*, 30 min (*10KS* and *10KP*) to obtain an ER membrane fraction, and the remaining supernatant was centrifuged at 191,065 × *g* for 30 min (*54KS* and *54KP*) to obtain ER-derived vesicles. Supernatants and membranes were solubilized in lysis buffer and resolved on SDS-PAGE, and ERGIC-53, BiP, Giantin, DIC, and tubulin localization was determined by Western blot analysis. A representative blot is shown ($n = 3$). *B*, cells as in *A* were nonspecifically or DHC1-silenced and were treated as in *A*, and ERGIC-53 movement into high-speed vesicles pellets was assessed. A representative blot of the 10 min recovery is shown ($n = 3$).

or DHC1-silenced cells were treated with BFA for 30 min to collapse the Golgi and move all ERGIC-53 into the ER. BFA was removed, and the movement of ERGIC-53 into vesicles was assessed by Western blot. 10 minutes after removal of BFA, most ERGIC-53 was found in the high-speed pellet in nonspecifically silenced cells. In contrast, little ERGIC-53 was found in the high-speed pellet in Mon1a-silenced cells (Fig. 8*A*). Similarly, the Golgi marker Giantin was found in the high-speed pellet in nonspecifically silenced cells, but a reduced amount was present in the high-speed pellet from Mon1a-silenced cells. These data support a role for Mon1a in the formation of vesicles at ERES. We note that BiP was found in all samples, but was most predominant in the 10,000 pellet, as would be predicted for an ER marker. We also note a slight tubulin contamination in the high-speed pellet at 10 min; however, this tubulin was present in all silenced samples. DIC, which associates with many types of vesicles, remained associated with the vesicle fraction in Mon1a-silenced cells, as expected. Silencing of DHC1 did not affect the ability of ERGIC-53 to be incorporated into high-speed pelleted vesicles (Fig. 8*B*). This suggests that dynein is required for efficient anterograde trafficking, but is dispensable in vesicle formation at ERES.

DISCUSSION

Mon1a was identified initially through a genetic screen as a gene that affected the localization and trafficking of cell surface and secreted proteins (9). A naturally occurring mutant allele of Mon1a resulted in increased movement of the mammalian iron transporter ferroportin through the secretory pathway. In this current study, we determined that reductions in Mon1a delay the reformation of the Golgi apparatus after BFA disruption and that Mon1a functions in efficient movement of molecules

from the ER to the Golgi and from the Golgi to the plasma membrane. We further determined that Mon1a interacts with DIC in the dynein-dynactin complex to efficiently generate ER-derived ERGIC-53-positive vesicles.

Initial studies in *S. cerevisiae* and *C. elegans* suggested that YMon1 and SAND-1, respectively, are involved in the endocytic pathway; however, the precise step in the endocytic pathway is different (1, 3, 4, 29). Based upon those studies and the sequence homology with YMon1, we expected that Mon1a would also function in the endocytic pathway. Surprisingly, reductions in Mon1a levels did not affect endocytosis, phagocytosis, or trafficking through the endocytic pathway. Additionally, the steady state size of organelles in the endocytic pathway was not affected by reduced levels of Mon1a. A recent study proposed that SAND-1 in *C. elegans* acts in ingestion of apoptotic cell corpses, a specific phagocytic event, and that mammalian Mon1a and Mon1b might have a similar function acting in complex with a mammalian homologue of Ccz1 (c7orf28b) (7). The *S. cerevisiae* homologues Mon1 and Ccz1 have been shown to be involved in autophagy (29). We previously reported that loss of Mon1a in macrophages did not affect erythrophagocytosis (9), consistent with the report by Kinchen and Ravichandran (7) that silencing of mammalian Mon1a or its homologue Mon1b did not affect phagocytosis. In the *C. elegans* study, silencing of both Mon1a and Mon1b, however, did affect acidification of the apoptotic cell-containing phagosome. A second role for Mon1a in the endocytic pathway was suggested by Poteryaev *et al.* (5). These authors proposed that SAND-1/Mon1a/b functions in endosome maturation by acting as a switch from Rab5-to-Rab7-positive endosomes (8). The authors noted that effects on the endocytic pathway were best seen when both Mon1a and Mon1b protein levels were reduced. Confirmatory results were reported in *S. cerevisiae* (17), supporting the role of Mon1 proteins in the endocytic pathway. Importantly, none of these studies reported whether loss of Mon1a, Mon1b, or SAND-1 affected vesicle trafficking in the secretory pathway.

We provide evidence that reductions in Mon1a affect transfer of vesicular contents from ER to Golgi and from Golgi to plasma membrane. Further, reduced levels of Mon1a lead to delayed assembly of the Golgi apparatus following BFA treatment. If Mon1a is required for ER-to-Golgi trafficking, one might expect that Golgi markers and the apparatus would be found more localized with the ER in Mon1a-silenced cells, as is seen in point mutants in Sec24 or Sar1 proteins (20, 30). This is not the case; reductions in Mon1a give rise to subtle but consistent changes in the morphology of the Golgi apparatus with longer extensions and less tight stacking of the Golgi. These results can be explained either by the fact that siRNA is not complete or by the fact that Mon1a also acts in retrograde trafficking from Golgi to ER. Studies are currently underway to address the role of Mon1a in retrograde trafficking to the ER.

Loss of Mon1a affects the generation of ER-derived ERGIC-53-positive vesicles. We show that Mon1a interacts with cytoplasmic DIC, which has been previously shown to be involved in trafficking at ER exit sites (23, 24). We observed that reductions in dynein result in Golgi fragmentation, but we did not see any diminution in ERGIC-53-positive vesicle formation. That

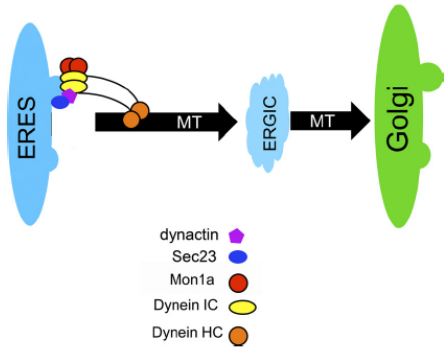

FIGURE 9. **Model of Mon1a and dynein acting in vesicle formation off the ER.** A model showing dynein-dynactin complex interacts with vesicles through the DIC and with microtubules (*MT*) through the DHC1. Dynein-dynactin interacts with Sec23 on the ERES (25). Mon1a interacts with dynein to efficiently traffic vesicles from ER to Golgi. *IC*, intermediate chain; *HC*, heavy chain.

dynein is involved in trafficking at ERES is not surprising. What is novel is the identification of Mon1a as a dynein-interacting protein that is important in efficient trafficking out of the ER. Reductions in Mon1a or DHC1 did not affect the ability to recruit Sec31 to ER exit sites, suggesting that Mon1a and DHC1 are recruited after COPII proteins. The dynein-dynactin complex then interacts with microtubules to efficiently guide vesicles and move them to the ERGIC and subsequently to the Golgi. A recent review by Zanetti *et al.* (31) suggests that vesicle formation at ERES remains to be further characterized. We propose a model where Mon1a is functioning at ER exit sites to assist in vesicle formation, that the dynein-dynactin complex binds to microtubules, Sec23, and Mon1a at ER exit sites, and that DIC binds Mon1a to efficiently traffic vesicles away from the ER (Fig. 9). Microtubules and motor proteins, including the dynein-dynactin complex, are clearly involved in trafficking. Perhaps Mon1a is an accessory protein that may act to stabilize the formation of vesicles exiting the ERES.

A finding that loss of Mon1a affects ER-to-Golgi membrane traffic does not preclude a role for Mon1a in other forms of vesicular traffic; in fact, we have shown that reductions in Mon1a can affect Golgi-to-plasma membrane sorting as well. As suggested by others, the SAND-1 family of proteins may be involved in many trafficking events (1, 3, 4, 7, 8, 17, 29). Indeed, many vesicle trafficking events require dynein and dynein-interacting proteins, possibly Mon1a. The finding that reduced levels of Mon1a in mammalian cells affects trafficking through the secretory apparatus may also be reconciled by studies that show that loss of SAND-1 affects autophagy in *C. elegans* (7). Studies in *S. cerevisiae* have shown that components of the secretory pathway including Sec1, Sec12, Sec16, and Sec23 are required for autophagy (32, 33). These studies suggest that the ER, and not the specific COPII vesicle components, is necessary for autophagosome formation by providing membrane (33, 34). It is possible that the effects on the ingestion of apoptotic cell corpses seen in *C. elegans* SAND-1 mutants or in mammalian cells silenced for Mon1a and its homologue Mon1b may reflect a common defect at the level of the secretory pathway. Why

vertebrates have two Mon1 proteins remains to be determined. Outside of the SAND domain of mammalian Mon1a and Mon1b, the homology of the two mammalian Mon1 proteins is less conserved. It is possible that these two proteins function in completely different membrane trafficking pathways. Studies are underway to further characterize how Mon1a interacts with dynein and whether there are other molecules that play a role in efficient intracellular vesicle trafficking.

Acknowledgments—We express our appreciation to members of the Kaplan/Ward laboratory for editing this manuscript.

REFERENCES

1. Wang, C. W., Stromhaug, P. E., Kauffman, E. J., Weisman, L. S., and Klionsky, D. J. (2003) Yeast homotypic vacuole fusion requires the Ccz1-Mon1 complex during the tethering/docking stage. *J. Cell Biol.* **163,** 973–985
2. Hoffman-Sommer, M., Kucharczyk, R., Piekarska, I., Kozlowska, E., and Rytka, J. (2009) Mutations in the *Saccharomyces cerevisiae* vacuolar fusion proteins Ccz1, Mon1, and Ypt7 cause defects in cell cycle progression in a num1Δ background. *Eur. J. Cell Biol.* **88,** 639–652
3. Kucharczyk, R., Hoffman-Sommer, M., Piekarska, I., von Mollard, G. F., and Rytka, J. (2009) The *Saccharomyces cerevisiae* protein Ccz1p interacts with components of the endosomal fusion machinery. *FEMS Yeast Res.* **9,** 565–573
4. Hoffman-Sommer, M., Migdalski, A., Rytka, J., and Kucharczyk, R. (2005) Multiple functions of the vacuolar sorting protein Ccz1p in *Saccharomyces cerevisiae*. *Biochem. Biophys. Res. Commun.* **329,** 197–204
5. Poteryaev, D., and Spang, A. (2005) A role of SAND family proteins in endocytosis. *Biochem. Soc. Trans.* **33,** 606–608
6. Poteryaev, D., Fares, H., Bowerman, B., and Spang, A. (2007) *Caenorhabditis elegans* SAND-1 is essential for RAB-7 function in endosomal traffic. *EMBO J.* **26,** 301–312
7. Kinchen, J. M., and Ravichandran, K. S. (2010) Identification of two evolutionarily conserved genes regulating processing of engulfed apoptotic cells. *Nature* **464,** 778–782
8. Poteryaev, D., Datta, S., Ackema, K., Zerial, M., and Spang, A. (2010) Identification of the switch in early-to-late endosome transition. *Cell* **141,** 497–508
9. Wang, F., Paradkar, P. N., Custodio, A. O., McVey Ward, D., Fleming, M. D., Campagna, D., Roberts, K. A., Boyartchuk, V., Dietrich, W. F., Kaplan, J., and Andrews, N. C. (2007) Genetic variation in *Mon1a* affects protein trafficking and modifies macrophage iron loading in mice. *Nat. Genet.* **39,** 1025–1032
10. Ryan, S. D., Bhanot, K., Ferrier, A., De Repentigny, Y., Chu, A., Blais, A., and Kothary, R. (2012) Microtubule stability, Golgi organization, and transport flux require dystonin-a2-MAP1B interaction. *J. Cell Biol.* **196,** 727–742
11. Perou, C. M., and Kaplan, J. (1993) Chediak-Higashi syndrome is not due to a defect in microtubule-based lysosomal mobility. *J. Cell Sci.* **106,** 99–107
12. Zhang, Y., Zolov, S. N., Chow, C. Y., Slutsky, S. G., Richardson, S. C., Piper, R. C., Yang, B., Nau, J. J., Westrick, R. J., Morrison, S. J., Meisler, M. H., and Weisman, L. S. (2007) Loss of Vac14, a regulator of the signaling lipid phosphatidylinositol 3,5-bisphosphate, results in neurodegeneration in mice. *Proc. Natl. Acad. Sci. U.S.A.* **104,** 17518–17523
13. Raiborg, C., Bremnes, B., Mehlum, A., Gillooly, D. J., D'Arrigo, A., Stang, E., and Stenmark, H. (2001) FYVE and coiled-coil domains determine the specific localization of Hrs to early endosomes. *J. Cell Sci.* **114,** 2255–2263
14. de Renzis, S., Sönnichsen, B., and Zerial, M. (2002) Divalent Rab effectors regulate the subcompartmental organization and sorting of early endosomes. *Nat. Cell Biol.* **4,** 124–133
15. Durchfort, N., Verhoef, S., Vaughn, M. B., Shrestha, R., Adam, D., Kaplan, J., and Ward, D. M. (2012) The enlarged lysosomes in *beige*$_j$ cells result from decreased lysosome fission and not increased lysosome fusion. *Traffic* **13,** 108–119
16. Ward, D. M., Vaughn, M. B., Shiflett, S. L., White, P. L., Pollock, A. L., Hill, J., Schnegelberger, R., Sundquist, W. I., and Kaplan, J. (2005) The role of LIP5 and CHMP5 in multivesicular body formation and HIV-1 budding in mammalian cells. *J. Biol. Chem.* **280,** 10548–10555
17. Nordmann, M., Cabrera, M., Perz, A., Bröcker, C., Ostrowicz, C., Engelbrecht-Vandré, S., and Ungermann, C. (2010) The Mon1-Ccz1 complex is the GEF of the late endosomal Rab7 homolog Ypt7. *Curr. Biol.* **20,** 1654–1659
18. Altan-Bonnet, N., Sougrat, R., Liu, W., Snapp, E. L., Ward, T., and Lippincott-Schwartz, J. (2006) Golgi inheritance in mammalian cells is mediated through endoplasmic reticulum export activities. *Mol. Biol. Cell* **17,** 990–1005
19. Saraste, J., Palade, G. E., and Farquhar, M. G. (1986) Temperature-sensitive steps in the transport of secretory proteins through the Golgi complex in exocrine pancreatic cells. *Proc. Natl. Acad. Sci. U.S.A.* **83,** 6425–6429
20. Storrie, B., White, J., Röttger, S., Stelzer, E. H., Suganuma, T., and Nilsson, T. (1998) Recycling of Golgi-resident glycosyltransferases through the ER reveals a novel pathway and provides an explanation for nocodazole-induced Golgi scattering. *J. Cell Biol.* **143,** 1505–1521
21. Helenius, A., and Aebi, M. (2004) Roles of *N*-linked glycans in the endoplasmic reticulum. *Annu. Rev. Biochem.* **73,** 1019–1049
22. Presley, J. F., Cole, N. B., Schroer, T. A., Hirschberg, K., Zaal, K. J., and Lippincott-Schwartz, J. (1997) ER-to-Golgi transport visualized in living cells. *Nature* **389,** 81–85
23. Watson, P., Forster, R., Palmer, K. J., Pepperkok, R., and Stephens, D. J. (2005) Coupling of ER exit to microtubules through direct interaction of COPII with dynactin. *Nat. Cell Biol.* **7,** 48–55
24. Iyadurai, S. J., Robinson, J. T., Ma, L., He, Y., Mische, S., Li, M. G., Brown, W., Guichard, A., Bier, E., and Hays, T. S. (2008) Dynein and Star interact in EGFR signaling and ligand trafficking. *J. Cell Sci.* **121,** 2643–2651
25. Fromme, J. C., Orci, L., and Schekman, R. (2008) Coordination of COPII vesicle trafficking by Sec23. *Trends Cell Biol.* **18,** 330–336
26. Townley, A. K., Feng, Y., Schmidt, K., Carter, D. A., Porter, R., Verkade, P., and Stephens, D. J. (2008) Efficient coupling of Sec23-Sec24 to Sec13-Sec31 drives COPII-dependent collagen secretion and is essential for normal craniofacial development. *J. Cell Sci.* **121,** 3025–3034
27. Hauri, H. P., Kappeler, F., Andersson, H., and Appenzeller, C. (2000) ER-GIC-53 and traffic in the secretory pathway. *J. Cell Sci.* **113,** 587–596
28. Rowe, T., Aridor, M., McCaffery, J. M., Plutner, H., Nuoffer, C., and Balch, W. E. (1996) COPII vesicles derived from mammalian endoplasmic reticulum microsomes recruit COPI. *J. Cell Biol.* **135,** 895–911
29. Wang, C. W., Stromhaug, P. E., Shima, J., and Klionsky, D. J. (2002) The Ccz1-Mon1 protein complex is required for the late step of multiple vacuole delivery pathways. *J. Biol. Chem.* **277,** 47917–47927
30. Fromme, J. C., Ravazzola, M., Hamamoto, S., Al-Balwi, M., Eyaid, W., Boyadjiev, S. A., Cosson, P., Schekman, R., and Orci, L. (2007) The genetic basis of a craniofacial disease provides insight into COPII coat assembly. *Dev. Cell* **13,** 623–634
31. Zanetti, G., Pahuja, K. B., Studer, S., Shim, S., and Schekman, R. (2012) COPII and the regulation of protein sorting in mammals. *Nat. Cell Biol.* **14,** 20–28
32. Ishihara, N., Hamasaki, M., Yokota, S., Suzuki, K., Kamada, Y., Kihara, A., Yoshimori, T., Noda, T., and Ohsumi, Y. (2001) Autophagosome requires specific early Sec proteins for its formation and NSF/SNARE for vacuolar fusion. *Mol. Biol. Cell* **12,** 3690–3702
33. Hamasaki, M., Noda, T., and Ohsumi, Y. (2003) The early secretory pathway contributes to autophagy in yeast. *Cell Struct. Funct.* **28,** 49–54
34. Di Bartolomeo, S., Corazzari, M., Nazio, F., Oliverio, S., Lisi, G., Antonioli, M., Pagliarini, V., Matteoni, S., Fuoco, C., Giunta, L., D'Amelio, M., Nardacci, R., Romagnoli, A., Piacentini, M., Cecconi, F., and Fimia, G. M. (2010) The dynamic interaction of AMBRA1 with the dynein motor complex regulates mammalian autophagy. *J. Cell Biol.* **191,** 155–168

CHAPTER 3

MON1A AND FCHO2 ARE REQUIRED FOR GOLGI ARCHITECTURE MAINTENANCE

3.1 Introduction

Mon1 is an evolutionarily conserved protein involved in membrane trafficking (1-3). Yeast Mon1 is a cytosolic protein recruited to the vacuole and is required for all fusion events involving the vacuole, including autophagy, cytoplasm to vacuole targeting (Cvt), and multivesicular body (MVB) pathways (4-6). In the nematode *Caenorhabditis elegans,* Mon1 is required for Rab7 activity, which is necessary for the transition from early to late endosomes (7). Mammals have two homologues of Mon1, Mon1a and Mon1b, which share less than 50% similarity at the amino acid level. In *C. elegans,* these Mon1 homologues may also be involved in endosome maturation. At endosomes, Mon1 is thought to displace the activator of Rab5, Rabex5, allowing for the recruitment of Rab7 to endosomal surfaces, thus permitting maturation to a late endosomal compartment (3). Reduction in Mon1a or Mon1b levels alone had no reported effect on endosomal morphology or maturation. However, reductions in both Mon1a and Mon1b showed an increase in the size of the Rab5 compartment and a concomitant decrease in the Rab7 endosomal compartment, suggesting an effect on endosomal maturation (3).

Mon1a had been identified as a modifier gene of splenic iron content with mice having different levels of splenic iron depending on the allele status of Mon1. The Mon1 allele in C57BL mice has a missense mutation, which led to higher cell surface levels of the iron exporter ferroportin and consequently a lower cellular iron content. Silencing studies in cultured cells demonstrated that RNAi-mediated depletion of Mon1a resulted in decreased expression of plasma membrane proteins and decreased protein secretion but had no discernable effect on endocytosis (8). Further studies demonstrated that Mon1a played a role in ER to Golgi traffic, as a reduction in Mon1a decreased ER vesicle formation. Protein interaction studies found that Mon1a associated with the microtuble (MT)-based motor Dynein and RNAi-mediated loss of either protein impaired ER to Golgi traffic (1).

Evidence that Mon1a acts at the ER, however, does not preclude it from having roles in other trafficking steps. Notably, reductions in Mon1a showed a mild morphological effect on the Golgi apparatus (1). Here we present data showing that severely reduced levels of Mon1a has a significant effect on Golgi morphology. Further, we show that Mon1a interacts with FCHo2, a protein involved in membrane bending and curvature stabilization at the plasma membrane. Our data suggest that FCHo2 is required for Golgi ribbon formation following mitosis.

3.2 Experimental Procedures

3.2.1 Mammalian cells and constructs. NIH3T3, Hela, and GalNAc-T2-GFP expressing Hela cells were maintained in DMEM with 10% FBS plus or minus 0.4 g/L G418 (Sigma-Aldrich, St. Louis, MO). GalNAc-T2-GFP Hela cells were a generous gift

from Dr. Brian Storrie (University of Arkansas). VSVGtsGFP were a generous gift from Dr. Jennifer Lippincott-Schwartz (National Institutes of Health). Mouse Mon1a was cloned into pCMV-Tag2BFLAG (Stratagene, La Jolla, CA) or pEGFPC1 (Clontech, Mountain View, CA). All constructs were sequence verified prior to use.

3.2.2 Transfections and Western analysis. HeLa, NIH3T3, or GalNAc-T2-GFP cells were plated onto tissue culture plates and allowed to grow for 24 to 48 h to 50-80% confluence. The cells were transfected with various constructs using Amaxa nucleofector technology (Lonza, Walkersville, MD) according to the manufacturer's directions. Protein expression was determined by solubilizing 2–4 x 10^6 cells in lysis buffer plus 2X protease inhibitor cocktail (Roche Applied Science, Boulder, CO). Samples were analyzed by SDS-PAGE and Western analysis was performed using either mouse anti-FLAG antibody (1:1000; Sigma-Aldrich, St. Louis, MO); rabbit anti-GFP (1:5000, ab6556; Abcam); mouse anti-tubulin (1:1000; GeneTex, San Antonio, TX) or mouse anti-Dyn-IC (1:2000, MMS-400R Covance, Princeton, NJ) followed by either peroxidase-conjugated goat anti-mouse immunoglobulin IgG (1:10,000; Jackson ImmunoResearch Laboratories, West Grove, PA) or peroxidase-conjugated goat anti-rabbit IgG (1:10,000; Jackson ImmunoResearch Labs, West Grove, PA). Antibodies to Mon1a and FCHo2 were generated as described (1). Rabbit anti-Mon1a and FCHo2 were used at a concentration of 1:100-500 followed by peroxidase conjugated goat anti-rabbit IgG (1:10,000) (Jackson ImmunoResearch Labs, West Grove, PA). The blots were developed using Western Lightning reagent (PerkinElmer Life Sciences, Waltham, MA). Tubulin was used as a loading control. All experiments were performed a minimum of three times and error bars represent the standard error of the mean.

3.2.3 Size exclusion chromatography. Cells expressing FLAG-tagged Mon1a were lysed in TBS pH 7.4 containing 0.1% Triton X-100 at 0°C for 45 min. The lysate was spun down at 14,000 RPM for 10 min and filtered through a 0.2-micron filter before running over a FPLC HiLoad 16/20 Superdex 200 prep grade column (Amersham Biosciences, Pittsburg, PA) at 0.5 mL/minute collecting 1 mL fractions. The analysis of FLAG-Mon1a presence in the FPLC fractions was resolved by SDS-PAGE and Western blot analysis.

3.2.4 Yeast two-hybrid (Y2H) and co-immunoprecipitation protein interaction studies. A Mon1a protein fragment containing the first 200 residues was used as a bait to screen a library of potential interacting partners in budding yeast as described previously (9). Cells were transfected with pFLAG-Mon1a or GFP-Mon1a, solubilized in lysis buffer, incubated 0ºC, 30 min, centrifuged at 10,000 x g, 10 min, immunoprecipitated using mouse anti-FLAG antibody (Sigma, St. Louis, MO) or rabbit anti-GFP (GeneTex, San Antonio, TX) and protein A/G-plus agarose (Santa Cruz Biotech, Santa Cruz, CA). Proteins in the immunoprecipitate were identified using Western blot analysis as described above (1).

3.2.5 Treatment with siRNA oligonucleotide pools. Cells were treated with nonspecific (NS), Mon1a (5'-UTR), Mon1a (ORF), FCHo2, Rab6a, or dynein heavy chain1-specific oligonucleotides (Dharmacon SiGenome SiRNA SMARTpool; Dharmacon RNA Technologies, Layfette, CO and University of Utah Sequencing Core; Salt Lake City, UT) using Oligofectamine Reagent (Invitrogen, Carlsbad, CA) according to the manufacturer's instructions as previously described (1). Briefly, 175,000 cells were treated with siRNAs in OptiMEM reduced-serum medium (Invitrogen, Carlsbad,

CA) for 6 h at 37°C before serum-replete medium was added for overnight growth. Cells were allowed to grow in DMEM with 10% FBS for 72 h before analyses were completed.

3.2.6 Brefeldin A treatment. Cells plated on glass coverslips were incubated with 5 μg/mL Brefeldin A (BFA) (Epicentre Biotechnologies, Madison, WI) for 30 min, washed three times, and placed in growth media for recovery. BFA recovery was visualized using an Olympus BX51 upright microscope with a 100X 1.4NA objective and Pictureframer software (Olympus, Melville, NY).

3.2.7 Epifluorescence and electron microscopy. Confocal images were captured on a Nikon A1R with the 488nm laser line and a 60x PLANAPO OIL immersion objective. Image analysis was performed using Volocity software as previously described (1). For electron microscopy (EM), cells were fixed in 2.5% glutaraldehyde/1% paraformaldehyde and transmission EM images capture at the University of Utah EM Core as previously described (1).

3.2.8 FRAP analysis. Cell transfected with siRNAs for nonspecific or FCHo2 were analyzed for lateral diffusions and membrane fusion of Golgi GalNAc-T2-GFP by photobleaching and recovery. FRAP was performed using a Nikon A1R with the 488nm laser line and a 60X PLANAPO OIL immersion objective. Regions of interest were selected for photobleaching and after three initial frames, 100% laser power was applied to these regions for 2 seconds, followed by time-lapse imaging of the recovery at one frame a second for 5 min.

3.3 Results

3.3.1 Mon1a interacts with the F-BAR protein FCHo2. We demonstrated that Mon1a is required for efficient anterograde trafficking in the secretory pathway due to its interaction with the microtubule-based molecular motor Dynein (1). A yeast two-hybrid (Y2H) screen was performed to identify interacting partners of Mon1a to give us insight into Mon1a function. A protein fragment containing the first 200 residues of Mon1a, used as bait, was found to interact with five different proteins (**Table 3.1**). We focused on one protein, the endocytosis effector FCHo2, as it was found from three different mammalian libraries and is known to function in membrane trafficking. FCHo2 is a F-BAR domain-containing protein that functions at the cell-surface as part of the machinery

Table 3.1 Yeast two-hybrid (Y2H) analysis of Mon1a binding partners

Bait	**Amino acids**	**Prey**	**a.a. cords.**	**Library**
Mon1a (*Hs*)	1-200	FCHo2	13-177	Macrophage
Mon1a (*Hs*)	1-200	FCHo2	7-106	Spleen
Mon1a (*Hs*)	1-200	FCHo2	14-150	Brain
Mon1a (*Hs*)	1-250	DPY30(99)	36-100	Macrophage
Mon1a (*Hs*)	1-200	FYN(537)	97-219	Brain
Mon1a (*Hs*)	1-200	LYN(582)	78-276	Spleen
Mon1a (*Hs*)	1-200	TXN	-18-106	Spleen

A yeast two-hybrid screen was performed using human Mon1a as bait. The first 200 amino acids of Mon1a was shown to interact with the clathrin-dependent endocytosis effector FCHo2. This interaction was seen in multiple independent libraries constructed from macrophages, spleen, and brain tissues. Mon1a was also shown to physically associate with Dpy30-like protein (99), a protein thought to be involved in the methylation of histones, tyrosine-protein kinases Fyn and Lyn, thought to be involved in several biological processes including cell growth and activation, respectively, as well as thioredoxin (Txn), which is required for cellular redox signaling.

necessary for clathrin-dependent endocytosis (10). The yeast two-hybrid result was corroborated by size exclusion chromatography and coimmunoprecipitation. Lysates from cells over-expressing functional FLAG-tagged Mon1a protein were passed over a size-exclusion column. Mon1a is predicted to be a 62 kDa protein, yet the majority of Mon1a migrated in two distinct sets of fractions that were about 150 kDa and in the void volume, which contains molecules greater than 330 kDa. This result suggests that Mon1a associates with other proteins as a higher molecular weight complex (**Figure 3.1A**). Mon1a was found in fractions the size consistent for Mon1a interacting with itself as a dimer (~150 kDa). To address the possibility of Mon1a dimerization, FLAG- and GFP-tagged Mon1a were co-expressed in NIH3T3 cells, GFP-Mon1a was immunoprecipitated, and the presence of FLAG-tagged Mon1a assessed by Western blot. Mon1a dimerization was confirmed, as GFP-Mon1a was able to pull down FLAG-Mon1a (**Figure 3.1B**). This interaction was specific as free GFP was unable to co-immunoprecipitate FLAG-Mon1a. To address whether Mon1a interacts with FCHo2, FLAG-Mon1a was immunoprecipitated from the high molecular weight FPLC fraction and the immunoprecipitate examined for the presence of FCHo2. FLAG-Mon1a interacted with endogenous FCHo2 as well as Dynein, a protein known to interact with Mon1a (**Figure 3.1C**) (1). FLAG-tagged Mon1a migrated in a void volume fraction consistent with a higher-order protein complex (**Figure 3.1A**). These results support an association between Mon1a and FCHo2 but do not distinguish if this interaction is direct or indirect. Our previous studies demonstrated that endocytosis was seemingly undisrupted in Mon1a deficient cells; however, a role for FCHo2 in the secretory pathway where Mon1a is known to function has yet to be addressed (1).

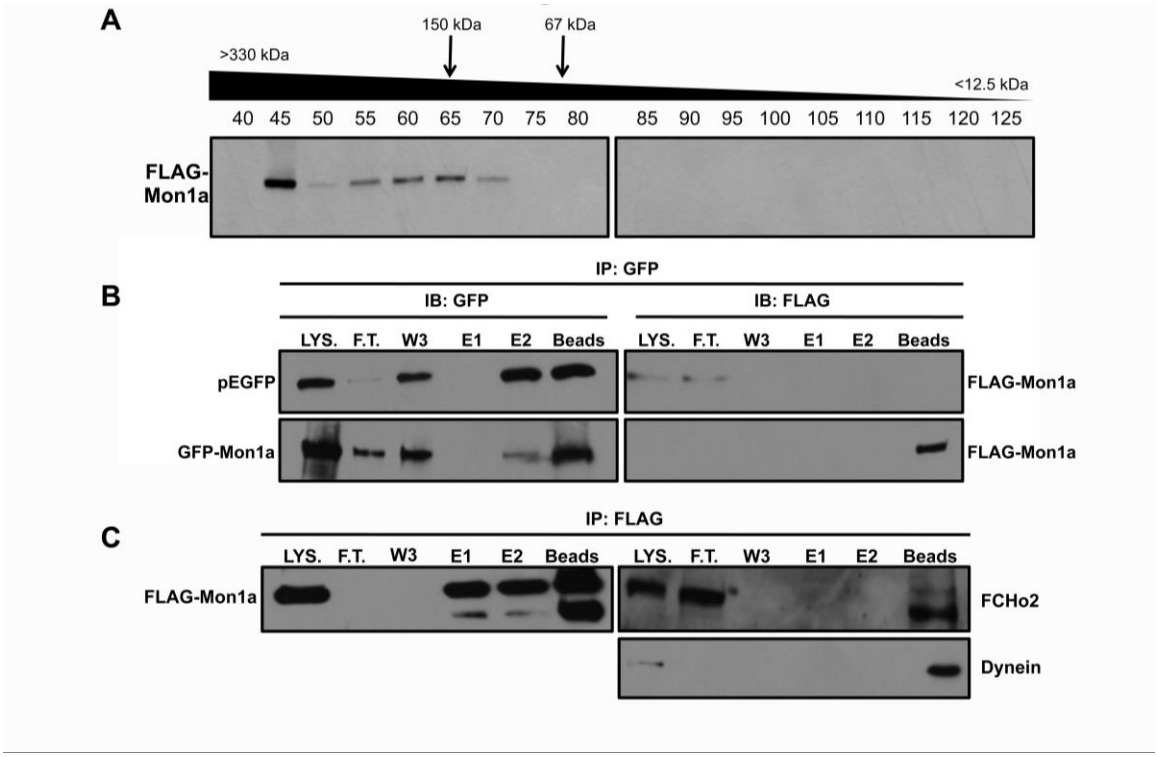

Figure 3.1 Mon1a dimerizes and associates with the endocytic F-BAR domain protein FCHo2 A. NIH3T3 cells were transfected by FLAG-Mon1a before lysing in the presence of 0.1% Triton X-100. Whole cell lysates were passed through a filter before injecting over a FPLC size-exclusion column. Fractions were resolved by SDS-PAGE and Western analysis using mouse anti-FLAG antibodies. B. pEGFP, GFP-, and FLAG-Mon1a constructs were co-expressed in NIH3T3 cells and lysed. Lysates were incubated with a GFP antibody and A/G-plus sephrose beads and samples were analyzed by SDS-PAGE and Western blot analysis for co-immunoprecipitation. C. Cells expressing FLAG-Mon1a were lysed and incubated with FLAG antibody and A/G-plus beads to immunoprecipitate FLAG-Mon1a. SDS-PAGE and Western analysis were done to confirm protein interactions.

3.3.2 FCHo2 is required for Golgi maintenance but not anterograde trafficking.

The Golgi complex resides at the center of the biosynthetic pathway, constantly receiving an input of newly synthesized proteins and lipids. We previously demonstrated that Mon1a depletion by siRNA alters the structure of the Golgi while leaving cisternae intact (1). To determine if FCHo2 has a role in the secretory pathway, we used siRNA to decrease FCHo2 levels in HeLa cells stably expressing GalNAc-T2-GFP, which is a

resident Golgi enzyme that labels the entirety of the Golgi apparatus (11,12). We observed organized perinuclear Golgi stacks with intact cisternae in cells transfected with nonspecific targeting siRNAs. In contrast, cells transfected with human FCHo2-specific siRNAs showed fragmented Golgi stacks. Golgi ribbons were disrupted but remained centrally clustered (**Figure 3.2A**). Notably, we assessed Golgi architecture in FCHo1-silenced cells, the FCHo2 homolog that also functions in clatherin-mediated endocytosis; however, Golgi remained intact so we focused our studies on FCHo2.

Confocal imaging was used to characterize further the breakdown of Golgi complex in FCHo2-depleted cells. Confocal images of cells transfected with nonspecific control siRNA showed tightly organized Golgi stacks at the perinucleus. In contrast, FCHo2-silenced cells presented fragmented Golgi, which was quantified using Volocity software to measure the GalNAc-T2-GFP signal in three-dimensional space on a cell-by-cell basis (1). The number of Golgi elements (GalNAc-T2-GFP+) was dramatically increased in FCHo2 silenced cells compared to nonspecifically siRNA transfected control cells (**Figure 3.2B**). Measurements of FCHo2-depleted cells demonstrated a bimodal distribution of surface area to volume for Golgi fragments, with a significantly increased number of Golgi fragments as compared to control cells, which showed intact uniformly sized Golgi (**Figure 3.2B**). Consistent with the confocal data and Volocity measurements, electron micrographs of cells with reduced levels of FCHo2 also showed severely fragmented Golgi phenotype. Cells showing less fragmented, individual mini-stacks lacking ribbon structures were also present. Control cells consistently displayed the canonical stacked cisternae (**Figure 3.2C**).

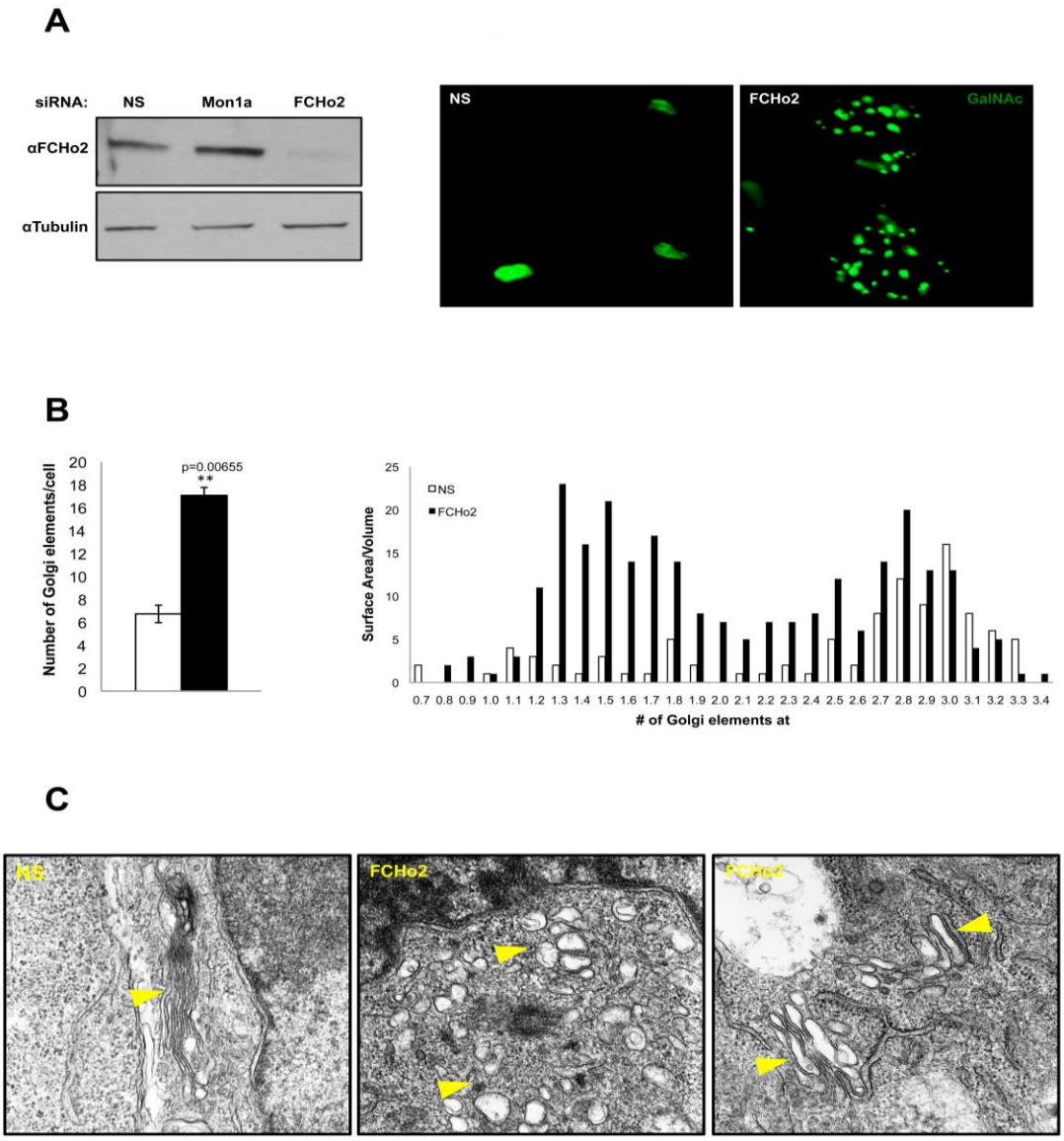

Figure 3.2 FCHo2 is required for maintenance of Golgi architecture A. HeLa cells expressing the Golgi protein GalNAc-T2-GFP were treated with siRNAs specific to FCHo2 or nonspecific control siRNAs for 72hrs. Western analysis was done to confirm efficient reduction of FCHo2. Golgi morphology was analyzed using live cell epifluorescence imaging of GalNAc-T2-GFP signal with a confocal microscope. B. Cells silenced as in (A) were imaged using confocal microscopy and images, specifically the Golgi channel, were quantified using Volocity software as described previously (1). Data are expressed as Golgi elements/cell or average Golgi surface area/volume expressed as voxels. C. Cells silenced as in (A) for nonspecific control or FCHo2-specific siRNAs were processed for electron micrograph analysis at 72hrs RNAi-treatment. Representative images are shown.

We have shown that FCHo2 physically interacts with Mon1a, a protein that is known to function in anterograde trafficking within the secretory pathway. A role for FCHo2 in the secretory pathway, however, has yet to be described. Golgi fragmentation in FCHo2 silenced cells could result from a defect in the anterograde pathway (12,13). To address this question, HeLa cells expressing GalNAc-T2-GFP were transfected with FCHo2 siRNAs for 72 hours prior to treatment with the fungal metabolite Brefeldin A (BFA). BFA causes a dramatic redistribution of Golgi membrane to the ER (14). Removal of BFA by washing allows the Golgi to reassemble. Cells transfected with nonspecific control siRNA recovered Golgi stacks 2 h after BFA was removed (**Figure 3.3**). Since FCHo2-silenced cells recovered their fragmented Golgi with the same kinetics as control cells (**Figure 3.3**), we conclude that the disorganized architecture of the Golgi apparatus in FCHo2 depleted cells is not a result of disrupted ER-Golgi transport.

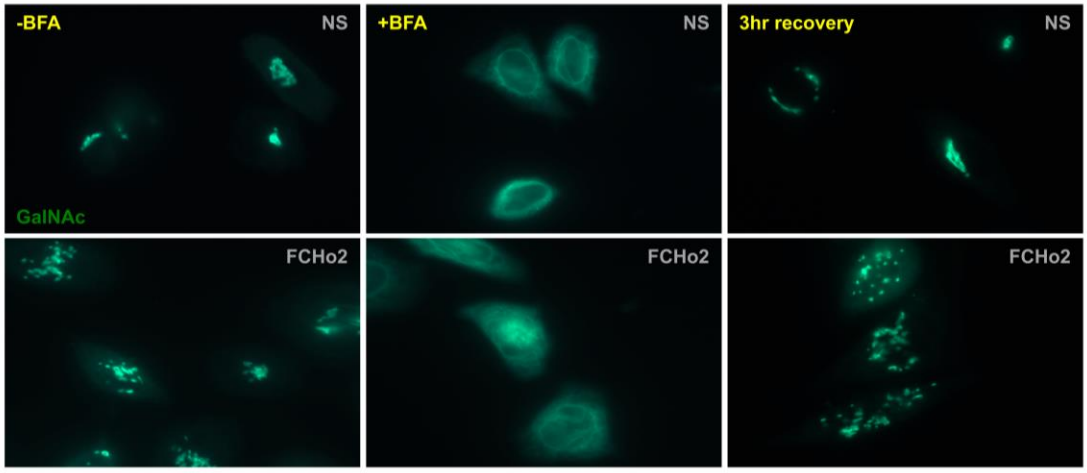

Figure 3.3 FCHo2 is not required for ER-Golgi transport HeLa cells stably expressing GalNAc-T2-GFP treated with siRNAs as described in Figure 2. Silenced cells were then incubated with BFA (5 µg/mL) for 30 min at 37°C before stringent washing. Movement from ER to Golgi was assessed at indicated time points by live cell epifluorescence microscopy.

3.3.3 siRNA targeting Mon1a (5'-UTR) results in Golgi fragmentation. One limitation of protein depletion through siRNA targeting is that RNAi can decrease mRNA and protein levels but cannot completely eliminate the expression of a target protein (15). RNAi oligos vary dramatically in inhibitory efficacy and the testing of a pool of oligos to a particular gene target is therefore commonly used to overcome this concern. Both Dynein and FCHo2 interact with Mon1a and fragment the Golgi apparatus when reduced by RNAi, yet Mon1a silencing only disorganizes the Golgi while leaving the cisternae intact (1). One hypothesis for this less severe Golgi phenotype is that Mon1a is required in both anterograde and retrograde trafficking at the ER-Golgi interface, which would likely preserve the architecture of the Golgi. Another possibility is that the residual Mon1a protein remaining after RNAi treatment is sufficient for Golgi complex maintenance. To test this latter possibility, RNAi oligos were designed to target either the open reading frame (ORF) or the 5'-untranslated region (5'-UTR) of Mon1a to test for differences in the efficiency of silencing between the two oligos. HeLa cells expressing GalNAc-T2-GFP were treated with each siRNA for 72 hours and Golgi morphology was assayed by epifluorescence microscopy. RNAi oligos specific to a sequence in the ORF of Mon1a led to the same Golgi phenotype as previously published, the Golgi was disorganized yet remained intact. Surprisingly, cells treated with oligos targeting the 5'-UTR of Mon1a led to fragmented Golgi stacks that were similar to that seen in FCHo2 silenced cells (**Figure 3.4A**). Rescue experiments were performed to confirm that this phenotype was specific to Mon1a protein depletion. Mon1a (5'-UTR) silenced cells were transfected with a FLAG-tagged mouse allele of Mon1a, which is RNAi-resistant. These cells were then assayed for Golgi morphology as well as ER-

Golgi trafficking that require Mon1a function. Compared to an empty vector control, Mon1a (5'-UTR) silenced cells expressing FLAG-Mon1a recovered both Golgi architecture and ER-Golgi trafficking comparable to nonspecifically silenced control cells, demonstrating that this new Golgi phenotype is specific to Mon1a protein suppression (**Figure 3.4B**). Electron micrograph analysis demonstrated that Mon1a protein suppression via RNAi resulted in a Golgi fragmentation strikingly similar to those seen in FCHo2 silenced cells (**Figure 3.4C**).

3.3.4 Co-depletion of Rab6 and FCHo2 or Mon1a (5'-UTR) suppresses silencing-induced Golgi fragmentation. The Golgi GTPase Rab6 and ER tether ZW10 function in vesicle fission and fusion, respectively, are required for the fidelity of membrane traffic and maintenance of Golgi morphology (12). Studies demonstrated that RNAi-dependent knockdown of the retrograde tether ZW10/RINT-1 resulted in a central clustering of Golgi fragments (12). This phenotype is strikingly similar to the Mon1a (5'-UTR) and FCHo2 knockdown-induced Golgi phenotypes. Rab6 is an evolutionarily conserved GTPase known to facilitate trafficking from the Golgi to the cell surface (anterograde), intra-Golgi transport mediated by the retrograde tether complex COG, and trafficking from the Golgi to the ER (retrograde) through a physical interaction with Dynein (12,16,17). Rab6 functions epistatic of ZW10, as co-silencing resulted in a Rab6 phenotype with intact Golgi architecture (12). We hypothesize that the Golgi fragmentation we observe in Mon1a (5'-UTR) and FCHo2 silenced cells requires the trafficking activity of Rab6. To test this possibility, GalNAc-T2-GFP expressing HeLa cells were treated with siRNA oligonucleotides, alone or in combination, specific to Mon1a (5'-UTR), FCHo2, or Rab6. Control and Rab6-depleted cells showed intact

Figure 3.4 siRNA targeting 5'-UTR of Mon1a fragments the Golgi apparatus GalNAc-T2-GFP expressing HeLa cells were transfected with siRNA specific to either the ORF or 5'-UTR of the Mon1a gene. A. Epifluorescence Golgi morphological analysis of Mon1a (ORF) versus (5'-UTR) silenced cells as compared to nonspecific control cells. B. Mon1a-silenced cells were transfected with FLAG-Mon1a or an empty vector control and Golgi morphology and ER-Golgi trafficking using a BFA recovery assessed by microscopy. C. siRNA transfected cells were fixed at 72 hours of silencing and ultrastructural analysis was performed. Representative electron micrographs are shown.

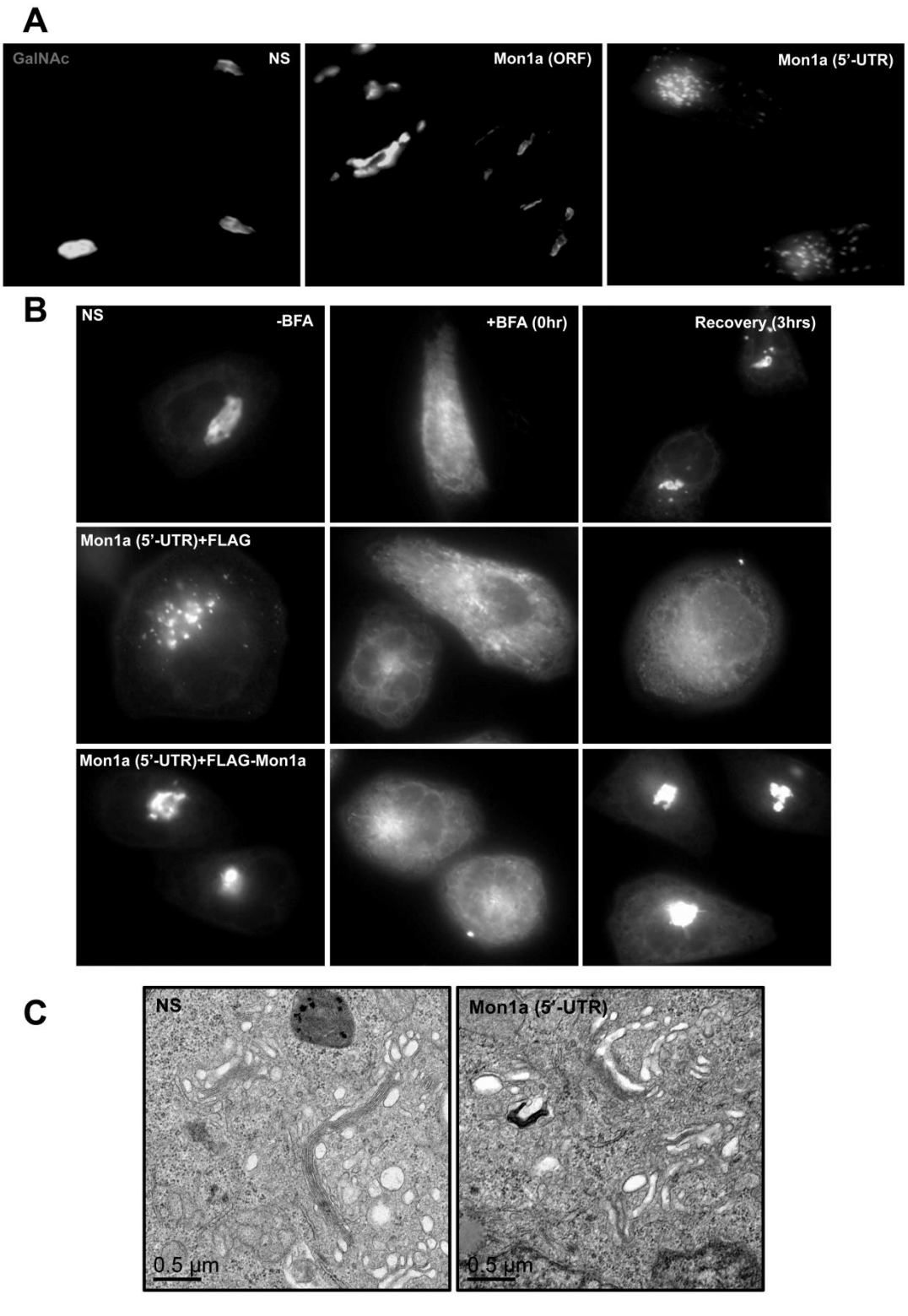
A
GalNAc
NS
Mon1a (ORF)
Mon1a (5'-UTR)
B
NS
-BFA
+BFA (0hr)
Recovery (3hrs)
Mon1a (5'-UTR)+FLAG
Mon1a (5'-UTR)+FLAG-Mon1a
C
NS
Mon1a (5'-UTR)
0.5 µm
0.5 µm

Golgi cisternae while Mon1a (5'-UTR) and FCHo2-silenced cells possessed fragmented Golgi elements as previously demonstrated (**Figure 3.5A**). Co-silencing of Rab6 and FCHo2 or Mon1a (5'-UTR) preserved the morphology of the Golgi stacks, resulting in a Rab6 silencing phenotype as opposed to a fragmented morphology. The percentage of cells showing Golgi fragmentation was quantified (**Figure 3.5B**). That depletion of Rab6a suppresses the effects of Mon1a and FCHo2 silencing suggests that Golgi fragmentation requires the function of the Golgi GTPase Rab6.

3.3.5 FCHo2 depletion does not affect vesicle traffic through the secretory pathway. Studies have shown that Golgi fragmentation does not necessarily impair secretion (23,26). Previously, we determined that reductions in Mon1a affected ER to Golgi and Golgi to plasma membrane (PM) trafficking (1). To determine if reductions in FCHo2 affect ER to Golgi and Golgi to PM trafficking, we took advantage of a temperature-sensitive allele of VSVGtsGFP that concentrates and restricts its localization to the ER at the restrictive temperature (39°C). Shifting cells to 32ºC allows cells to traffic VSVGtsGFP from ER to Golgi. Trafficking from ER to Golgi was unimpaired in FCHo2 silenced cells although the Golgi structures remained fragmented (**Figure 3.6A**). An intrinsic trait of all mammalian cells is that membrane traffic is temperature-sensitive. Incubation of cells at 20°C allows trafficking from the ER to the Golgi but no further. Silenced cells were transfected with VSVGtsGFP and incubated overnight at 39°C to restrict VSVGtsGFP to the ER. The analysis of FCHo2 function in Golgi-PM transport was done by allowing VSVGtsGFP to accumulate at the Golgi at 20°C. In control and FCHo2-depleted cells, the movement of VSVGtsGFP out of the Golgi to the cell surface was unimpaired at the permissive temperature (**Figure 3.6A**). These data strongly

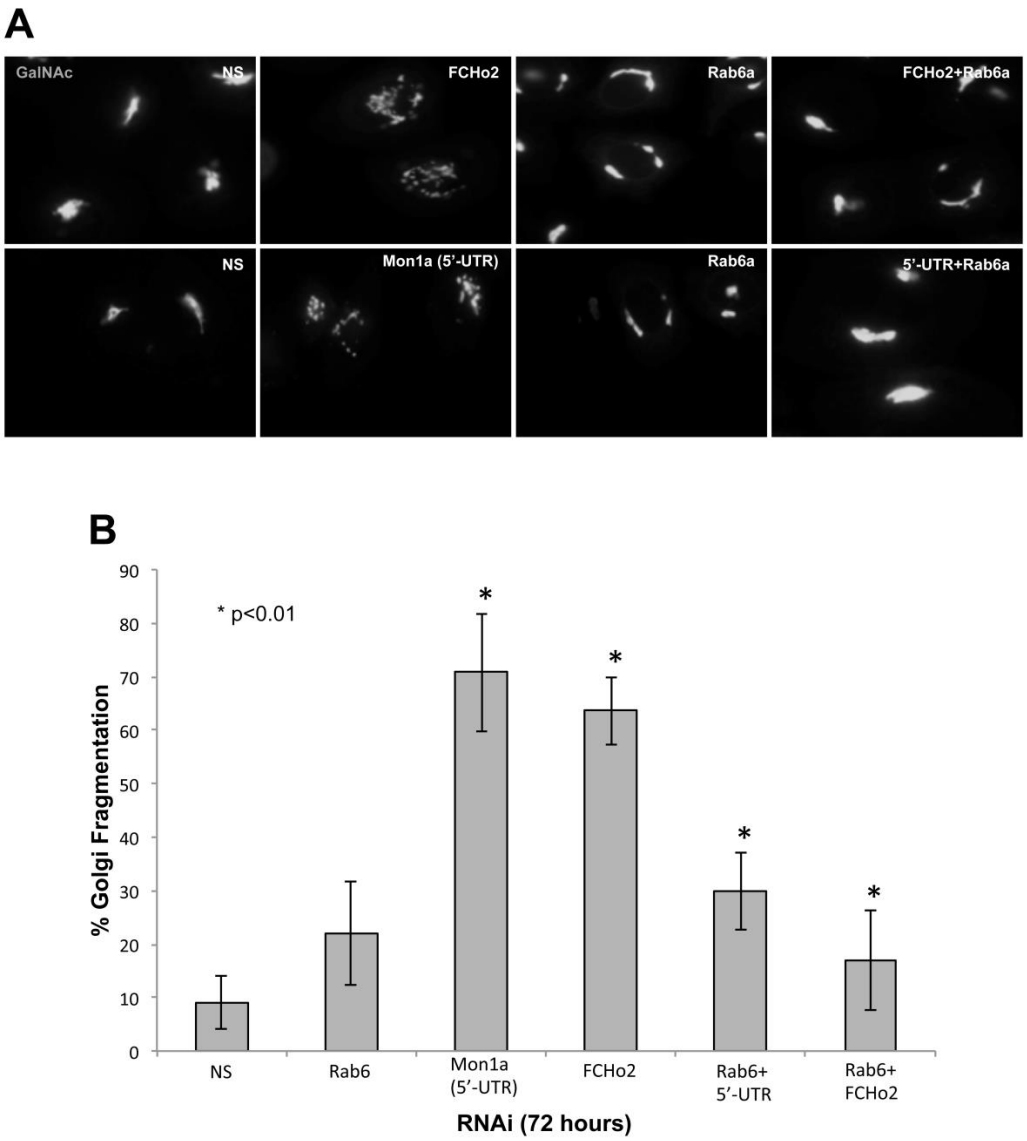

Figure 3.5 Mon1a (5'-UTR) and FCHo2 silencing-induced Golgi fragmentation requires Rab6 activity A. HeLa cells expressing GalNAc-T2-GFP were silenced with Mon1a (5'-UTR), FCHo2 or Rab6 alone or in combination for 72 hours. Epistasis was established by scoring Golgi morphology using live cell epifluorescence microscopy. B. Quantification of four independent epistasis experiments showing percent Golgi fragmentation with p values less than 0.01.

suggest that FCHo2 is not required in vesicle trafficking through the secretory pathway.

It is known that glycosylation of proteins can be impaired when properly organized Golgi architecture is broken down. Carbohydrate processing requires the sequential activity of a number of enzymes that span the entirety of the Golgi stack (26,27). N-acetyl-D-glucosamine is a rare, immature carbohydrate structure that is typically seen on cells where the sequential activity of glycosylation enzymes is disrupted through Golgi fragmentation (26). To determine if FCHo2 or Mon1a depletion disrupts proper glycosylation of proteins localized at the plasma membrane, silenced cells were placed at 0ºC and incubated with an Alexa594-conjugated lectin (GS-II) that binds the immature glycosylation mark N-acetyl-D-glucosamine of cell surface proteins. FCHo2 silenced cells had significantly increased GS-II binding at the cell surface while control cells had almost no GS-II fluorescence (**Figure 3.6B**). These data demonstrate that FCHo2 reduction disrupts Golgi architecture impairing proper glycosylation yet trafficking through the Golgi to the cell surface is uninhibited.

3.3.6 Golgi fragmentation in FCHo2-depleted cells is cell cycle-dependent. The mammalian Golgi apparatus consists of individual stacks of Golgi cisternae, termed "mini-stacks". Golgi membrane laterally link individual stacks through membrane tubules, creating Golgi "ribbons" (18-20). Golgi material must be partitioned between daughter cells during mitosis, which is facilitated through the systematic breakdown of Golgi ribbons to individual stacks and ultimately into vesicles. After cell division, the vesiculated Golgi coalesces and the organelle is reassembled independently in each daughter cell (19,20). Reductions in FCHo2 protein cause Golgi to fragment, presumably, into mini-stacks but not vesiculate. There are two likely possibilities that

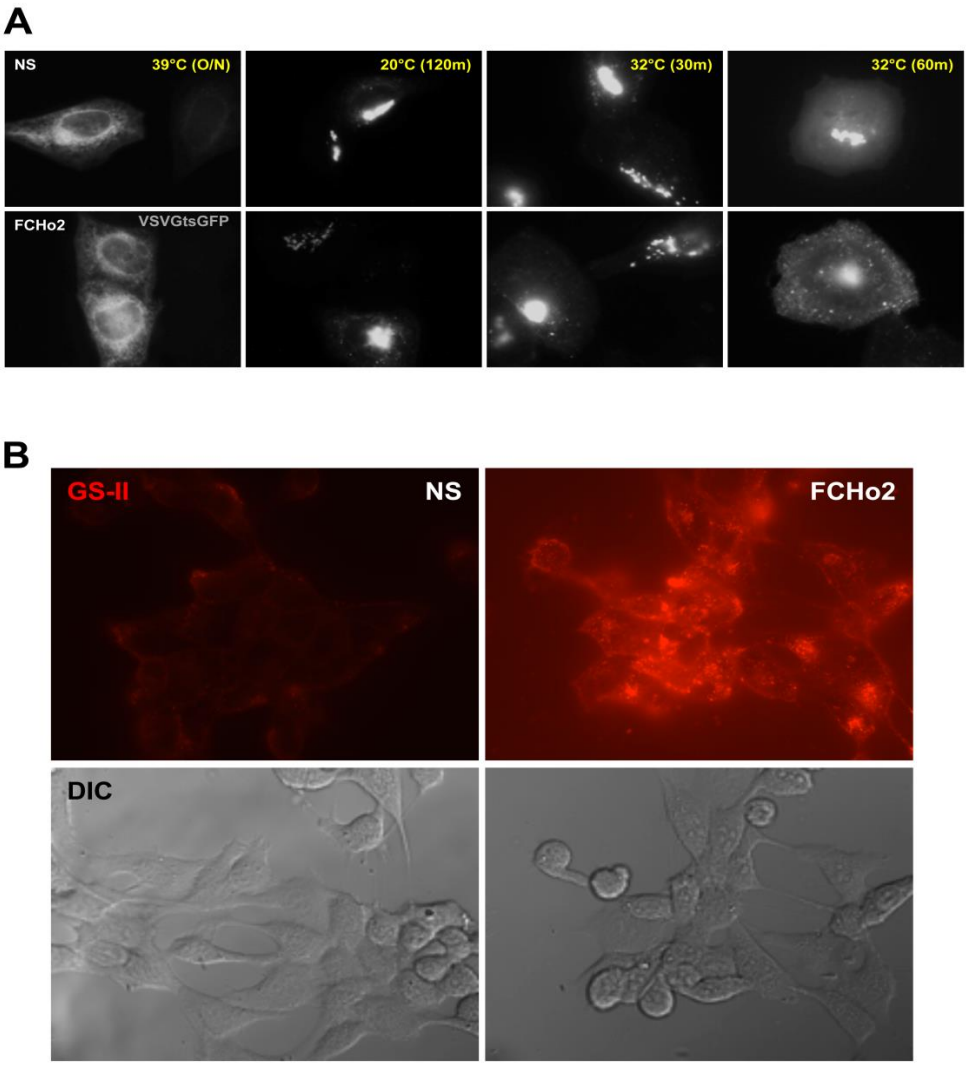

Figure 3.6 FCHo2-silenced cells show normal kinetics of Golgi to cell surface trafficking but increased immature glycosylation structures A. HeLa cells transfected with nonspecific or FCHo2-specific siRNA for 48 h and then cells were transfected with VSVGtsGFP and grown overnight at 39.5°C. Cells were shifted to 20°C for 2 h to allow VSVGtsGFP capture in the Golgi apparatus. Cells were then shifted to the permissive temperature (32ºC) and images captured at 30 and 60 min. B. Cells silenced as in (A) for 72 h were incubated at 4ºC with the cell impermeable Alexa594-conjugate GS-II lectin. Cells were extensively washed and epifluorescence images captured. Representative images are shown.

could give rise to this phenotype. First, mini-stack fragments in FCHo2-silenced cells may result from ribbon breakdown. Golgi ribbon maintenance may require membrane stabilization, which is a known activity of F-BAR domain family members. If FCHo2 is required for ribbon stability, then reducing FCHo2 levels should be sufficient to induce Golgi fragmentation. Alternatively, FCHo2 may act after mitosis when Golgi reformation occurs by actively tubulating Golgi membranes to link individual stacks and thus creating Golgi ribbons. F-BAR proteins like FCHo2 have been observed to cause massive membrane tubulation when highly expressed in cell culture (21,22), an activity presumably required in Golgi ribbon formation. RNAi and cell cycle arrest were utilized to address if FCHo2 or Mon1a activity were required in Golgi ribbon stability versus ribbon formation. Suppression of Golgi fragmentation by arresting the cell cycle in silenced cells would strongly suggest that FCHo2/Mon1a activity is required after mitosis in Golgi ribbon formation. To test this hypothesis, FCHo2 and Mon1a (5'-UTR) were knocked down using siRNA in cell cycle-arrested, GalNAc-expressing HeLa cells. Continued incubation in thymidine blocks cells at the G1/S phase, arresting the cell cycle before mitosis preventing Golgi disassembly. Control cells after 72 h of nonspecific silencing possessed tight, organized Golgi stacks in the presence or absence of thymidine (**Figure 3.7A**). As a control, we also silenced Dynein, which causes Golgi fragmentation into vesicles that presumably is not cell cycle-dependent. The presence or absence of thymidine did not alter the level of Golgi fragmentation observed in Dynein depleted cells. In contrast, the presence of thymidine in FCHo2-silenced cells in showed intact, organized Golgi stacks, whereas in the absence of thymidine treatment, the Golgi stacks in FCHo2-silenced cells were fragmented. This suggests that the FCHo2 silencing

phenotype is cell cycle-dependent. Golgi morphology was scored and quantified over several experiments and cell cycle arrest significantly suppressed FCHo2 silencing-induced Golgi fragmentation (**Figure 3.7B**). Mon1a (5'-UTR) treated cells showed a modest but not significant suppression of Golgi fragmentation in thymidine treated cells, suggesting that this phenotype is not cell cycle-dependent.

These cell cycle data strongly suggests that FCHo2 is required for the reassembly of the Golgi apparatus at the level of Golgi ribbon formation, which requires the fusion of Golgi membranes (23). The Golgi complex in mammalian cells is a dynamic structure where contents within cisternae are laterally mixed as the Golgi reassembles and ribbons form following mitotic events (19). The architecture of Golgi stacks is disrupted in cells with markedly reduced levels FCHo2 or Mon1a, but it is not known if there is communication between these fragmented Golgi elements through membrane fission and fusion events. We utilized fluorescence recovery after photobleaching (FRAP) (23-26) to determine if there is communication between Golgi elements in FCHo2 or Mon1a silenced cells. If FCHo2 or Mon1a are required for communication between Golgi fragments, then we expect that an individual Golgi element may not recover its fluorescence after photobleaching because unquenched fluorescence protein cannot be brought into the bleached structure. Nonspecifically, FCHo2 or Mon1a (5'-UTR) silenced GalNAc-T2-GFP expressing cells were imaged with epifluorescence confocal microscopy. A region of the Golgi structure was bleached and fluorescence recovery monitored. In control cells, fluorescence recovery occurred in a matter of seconds (**Figure 3.7C**). Conversely, recovery was completely blocked in FCHo2 and Mon1a

Figure 3.7 Golgi fragmentation in FCHo2-depleted cells is cell cycle-dependent A. GalNAc-T2-GFP expressing cells were transfected with siRNA nonspecific, FCHo2, or DHC1for 24 h before cell cycle arrest was achieved by 2 mM thymidine treatment for an additional 48 h. Golgi morphology was scored using epifluorescence microscopy with representative images shown. B. Quantifications of four independent experiments are graphed showing the percent of Golgi fragmentation with and without thymidine treatment. C. Cells treated with nonspecific, FCHo2, or Mon1a (5'-UTR) oligos for 72 h were visualized by live cell microscopy. Golgi elements (GalNAc-T2-GFP-positive) were photobleached and recovery assessed at indicated times by time-lapse microscopy.

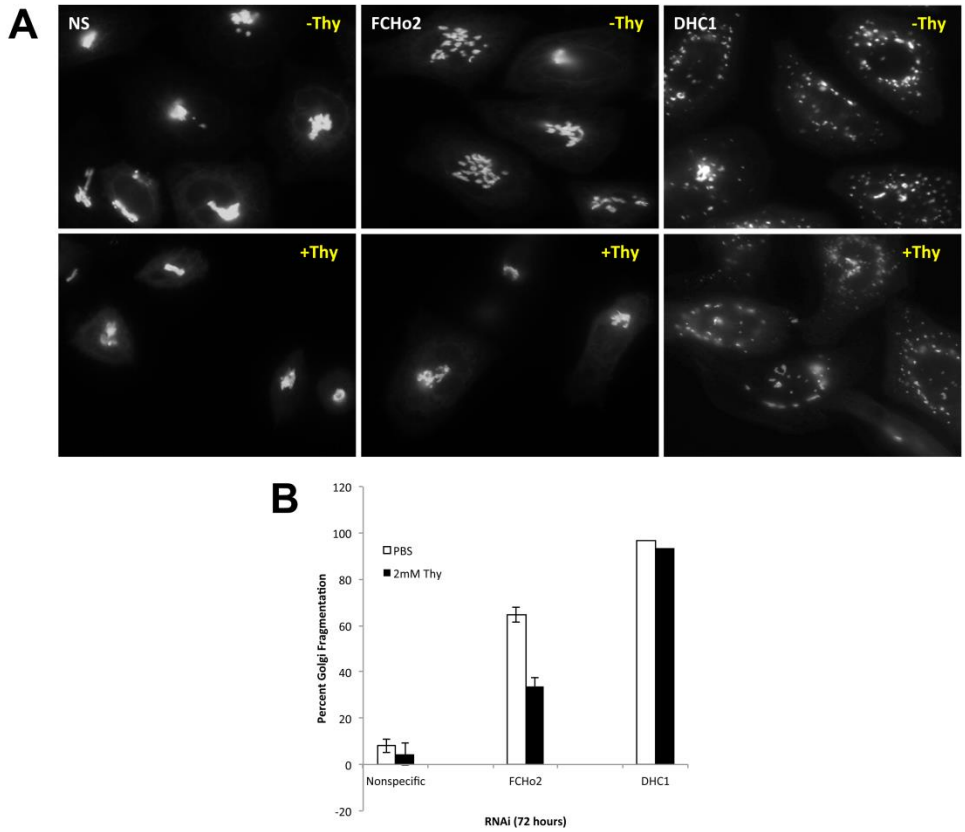
A
NS
-Thy
FCHo2
-Thy
DHC1
-Thy
+Thy
+Thy
+Thy
B
120
100
80
60
40
20
0
-20
PBS
2mM Thy
Percent Golgi Fragmentation
Nonspecific
FCHo2
DHC1
RNAi (72 hours)
C
NS
Pre-bleach
Bleach
60s recovery
5m recovery
Mon1a (5'-UTR)
FCHo2

silenced cells strongly suggesting that they function in membrane ribbon formation and Golgi communication.

3.4 Discussion

Our previous studies showed that Mon1a plays a role in ER-Golgi traffic (1). In this manuscript, we show that Mon1a is essential for maintaining Golgi integrity. Our previous study showed that Mon1a has a physical interaction with Dynein. Reductions in the levels of Mon1a or Dynein resulted in an impairment of vesicle formation and trafficking at the ER, respectively (1). Here we show that depletion of Mon1a or Dynein results in Golgi fragmentation. Epistasis experiments showed that silencing Rab6 influenced the Mon1a silencing phenotype, as Rab6 is required for the initial step of vesicle formation at the Golgi (12,17). This result is consistent with Mon1a's role at the ER in efficient vesicle generation. Interestingly, silencing Rab6 did not prevent the effect of reduced Dynein levels on Golgi morphology. The Golgi remained fragmented when Rab6 and Dynein were co-silenced. We hypothesize that ER-derived vesicle are generated at the ER but are not transported appropriately in Dynein silenced cells, resulting in Golgi fragmentation. Based on findings that the RNAi phenotypes are dependent on the degree of protein reduction, we infer that there is a greater requirement for Mon1a at ER-Golgi trafficking then in Golgi maintenance.

We identified FCHo2 as a Mon1a interacting protein. Silencing of Mon1a or FCHo2 results in Golgi fragments that remain centrally clustered likely around the microtubule-organizing center, the canonical site of Golgi assembly. In contrast, Dynein silencing leads to dispersed severely fragmented Golgi fragments (1). The effects of silencing Mon1a or FCHo2 are not identical. Both silencing phenotypes require the

activity of Rab6, but the effects of FCHo2 reduction are cell cycle-dependent. FCHo2 is a member of a large family of proteins known as F-BAR domain-containing proteins that are found in all eukaryotes, plants being the only exception. It is thought that 21 F-BAR genes encode about 36 proteins in humans, the majority of which have been demonstrated to function in endocytosis. FCHo2 was shown to bind to the plasma membrane and recruit protein machinery required for the formation of clathrin-coated pits, an initial step in endocytosis. This role in endocytosis requires the F-BAR domain of FCHo2 and its membrane bending capacity, suggesting that FCHo2 deforms the plasma membrane to initiate the site of clathrin-coated vesicle formation (10,21,22,28,29). Membrane bilayers that facilitate compartmentalization in all eukarya require protein machinery that can deform and induce membrane curvature that mediates organelle shaping and vesicle formation supporting intracellular communication (15,21,28-30). Members of the F-BAR domain family, including FCHo2, have been demonstrated to perform membrane tubulating activities *in vivo* and *in vitro*. The F-BAR domain is formed through an antiparallel dimerization of the amino-terminus of two FCHo2 proteins creating a curved module lined with positively charged residues that are thought to interact with the negatively charged phospholipid headgroups of membrane bilayers, ultimately facilitating membrane tubulation (28).

We hypothesize that FCHo2 is required to reform the Golgi ribbon after mitosis because prevention of mitosis through cell cycle arrest significantly decreases the Golgi fragmentation observed in FCHo2 silenced cells. This role is consistent with the identified role of FCHo2 as a membrane deforming protein (10,22). FCHo2 binding to the cell surface is mediated by phosphatidylinositol 4,5-bisphosphate (Ptd(4,5)P(2)),

which has been shown to be found at the plasma membrane but also at Golgi stacks (31). We have not yet identified FCHo2 at the Golgi ribbon, although the interaction is likely transient. We believe that FCHo2's capacity for membrane tubulation is focused at Golgi cisternae promoting Golgi reassembly and ribbon formation after mitotic events. Data showing that the loss of FCHo2 prevents the lateral transfer of Golgi membrane and material suggest that FCHo2 is required for Golgi ribbon formation, although the exact step of FCHo2 action remains to be clarified.

The sole Mon1 protein in yeast and nematodes is involved in endocytosis (4,5,7,32). In mammals, Mon1b appears to have retained the original function and has been shown to act at the transition from early to late endosomes (2,3). Mon1b was shown to inhibit Rabex5 an activator of Rab5, which displaced Rab5 from early endosomes. Subsequently, Mon1b was shown to be able to recruit Rab7 to endosomal surfaces through an interaction with the HOPS complex. Notably, both in overexpression and RNAi studies, Mon1a was only shown to have effects on endosomal maturation in combination with Mon1b and never by itself. Further, Mon1b was shown to interact with several subunits of the HOPS complex but Mon1a did not. Our studies have shown that loss of Mon1a had no effect on endocytosis but instead affected trafficking in the secretory pathway (1). While we can point to specific steps requiring Mon1a activity, we do not at this point know its precise biochemical function. Here we demonstrate that both Mon1a and FCHo2 interact physically and are needed for the proper maintenance of Golgi architecture.

3.5 References

1. Bagley, D. C., Paradkar, P. N., Kaplan, J., and Ward, D. M. 2012 *The Journal of biological chemistry* 287: 25577-25588

2. Kinchen, J. M., and Ravichandran, K. S. 2010 *Nature* 464: 778-782

3. Poteryaev, D., Datta, S., Ackema, K., Zerial, M., and Spang, A. 2010 *Cell* 141: 497-508

4. Wang, C. W., Stromhaug, P. E., Kauffman, E. J., Weisman, L. S., and Klionsky, D. J. 2003 *J Cell Biol* 163: 973-985

5. Wang, C. W., Stromhaug, P. E., Shima, J., and Klionsky, D. J. 2002 *J Biol Chem* 277: 47917-47927

6. Wang, X., Herberg, F. W., Laue, M. M., Wullner, C., Hu, B., Petrasch-Parwez, E., and Kilimann, M. W. 2000 *J Neurosci* 20: 8551-8565

7. Poteryaev, D., Fares, H., Bowerman, B., and Spang, A. 2007 *EMBO J* 26: 301-312

8. Wang, F., Paradkar, P. N., Custodio, A. O., McVey Ward, D., Fleming, M. D., Campagna, D., Roberts, K. A., Boyartchuk, V., Dietrich, W. F., Kaplan, J., and Andrews, N. C. 2007 *Nat Genet* 39: 1025-1032

9. Garrus, J. E., von Schwedler, U. K., Pornillos, O. W., Morham, S. G., Zavitz, K. H., Wang, H. E., Wettstein, D. A., Stray, K. M., Cote, M., Rich, R. L., Myszka, D. G., and Sundquist, W. I. 2001 *Cell* 107: 55-65

10. Henne, W. M., Boucrot, E., Meinecke, M., Evergren, E., Vallis, Y., Mittal, R., and McMahon, H. T. 2010 *Science* 328: 1281-1284

11. Rottger, S., White, J., Wandall, H. H., Olivo, J. C., Stark, A., Bennett, E. P., Whitehouse, C., Berger, E. G., Clausen, H., and Nilsson, T. 1998 *J Cell Sci* 111 (Pt 1): 45-60

12. Young, J., Stauber, T., del Nery, E., Vernos, I., Pepperkok, R., and Nilsson, T. 2005 *Mol Biol Cell* 16: 162-177

13. Palmer, K. J., Hughes, H., and Stephens, D. J. 2009 *Mol Biol Cell* 20: 2885-2899

14. Fujiwara, T., Oda, K., Yokota, S., Takatsuki, A., and Ikehara, Y. 1988 *J Biol Chem* 263: 18545-18552

15. 2003 *Nat Cell Biol* 5: 489-490

16. Del Nery, E., Miserey-Lenkei, S., Falguieres, T., Nizak, C., Johannes, L., Perez, F., and Goud, B. 2006 *Traffic* 7: 394-407

17. Matanis, T., Akhmanova, A., Wulf, P., Del Nery, E., Weide, T., Stepanova, T., Galjart, N., Grosveld, F., Goud, B., De Zeeuw, C. I., Barnekow, A., and Hoogenraad, C. C. 2002 *Nat Cell Biol* 4: 986-992

18. Vinke, F. P., Grieve, A. G., and Rabouille, C. 2011 *Biochem J* 433: 423-433

19. Tang, D., and Wang, Y. 2013 *Trends Cell Biol*

20. Wang, Y., and Seemann, J. 2011 *Cold Spring Harb Perspect Biol* 3: a005330

21. Frost, A., De Camilli, P., and Unger, V. M. 2007 *Structure* 15: 751-753

22. Henne, W. M., Kent, H. M., Ford, M. G., Hegde, B. G., Daumke, O., Butler, P. J., Mittal, R., Langen, R., Evans, P. R., and McMahon, H. T. 2007 *Structure* 15: 839-852

23. Koegler, E., Bonnon, C., Waldmeier, L., Mitrovic, S., Halbeisen, R., and Hauri, H. P. 2010 *Traffic* 11: 70-89

24. Sprague, B. L., and McNally, J. G. 2005 *Trends Cell Biol* 15: 84-91

25. Chen, Y., Lagerholm, B. C., Yang, B., and Jacobson, K. 2006 *Methods* 39: 147-153

26. Feinstein, T. N., and Linstedt, A. D. 2008 *Mol Biol Cell* 19: 2696-2707

27. Kellokumpu, S., Sormunen, R., and Kellokumpu, I. 2002 *FEBS Lett* 516: 217-224

28. Frost, A., Perera, R., Roux, A., Spasov, K., Destaing, O., Egelman, E. H., De Camilli, P., and Unger, V. M. 2008 *Cell* 132: 807-817

29. Frost, A., Unger, V. M., and De Camilli, P. 2009 *Cell* 137: 191-196

30. Futterer, K., and Machesky, L. M. 2007 *Cell* 129: 655-657

31. Watt, S. A., Kular, G., Fleming, I. N., Downes, C. P., and Lucocq, J. M. 2002 *Biochem J* 363: 657-666

32. Poteryaev, D., and Spang, A. 2005 *Biochem Soc Trans* 33: 606-608

CHAPTER 4

CONCLUSIONS AND FUTURE DIRECTIONS

The generation of the eukaryotic endomembrane system allowed biochemical processes to be compartmentalized with sophisticated spatial and temporal regulation (1-8). The endomembrane system required the development of protein machinery that allowed for the intracellular communication between these membrane-bound organelles. Significant strides have been made in understanding and identifying this machinery through model organisms, genetic screens, and biochemical techniques yet much of the actors and their roles in this system remain to be elucidated (9-12). Characterizing the endomembrane system and the proteome that regulates it is a central theme in cellular and molecular biology. The work described in this thesis addresses the characterization of a gene product, Mon1a, and the role it plays in membrane traffic and organelle maintenance within the mammalian secretory pathway.

4.1 Mon1a function in the secretory pathway

The fidelity of the secretory pathway relies on highly regulated trafficking of transport vesicles and their contents from a donor to an acceptor compartment (1-3,9,10,13-15). The cell biology axiom of ER-Golgi-PM outlining the secretory pathway relies on numerous effectors from coat proteins and GTPases to cytoskeletal elements and

molecular motors. Genetics first done in *S. cerevisiae* began to describe the mechanisms of membrane traffic in that cytosolic coat proteins are recruited to membrane surfaces via GTPases to initiate coat cage assembly and vesicle formation. Cytoskeletal motors then can interact with newly formed vesicles to transport them along cytoskeletal tracks to the next organelle depot (9-11). The original identification and characterization of Mon1 was performed in yeast where Mon1 was shown to function within the endocytic pathway at the vacuole (20,21). Recent studies on Mon1a, its homologue Mon1b, and nematode SAND1 have suggested that their function is evolutionarily conserved and is needed for proper maturation of endosomal compartments in higher eukaryotes (17-19). Yeast strains deleted for Mon1 present a range of phenotypes that include vacuole fragmentation, increased zinc sensitivity, and vacuolar hydrolase missorting (20,21).

The original characterization of mammalian Mon1a analyzed the regulation of iron stores in mice (22). This work demonstrated that the C57BL strains of mice carried an intrinsic "gain-of-function" mutation in Mon1a that results in more efficient trafficking within the secretory pathway, ultimately affecting cellular iron reserves. The authors provided evidence that C57BL mice have less iron in their cells as a direct result of having increased levels of the iron exporter ferroportin at the cell surface compared to other mouse strains. They went on to show that Mon1a function was not unique to ferroportin trafficking but affected all soluble and membrane-bound proteins that enter the secretory pathway. The aim of the second chapter of this thesis was to clarify the role of Mon1a in the secretory pathway in greater detail.

Biochemical and siRNA analysis revealed that Mon1a function affected the movement of proteins within the biosynthetic apparatus (16). As in yeast, Mon1a is a

cytosolic protein that is recruited to membrane surfaces. Cell fractionation studies using epitope-tagged Mon1a associated with organelles of the early secretory pathway, migrating coincidently with ER markers and to a lesser extent with the Golgi. Mon1a protein suppression through siRNA treatment demonstrated that Mon1a was required for efficient trafficking of proteins through the secretory apparatus at both early and late transport events. Mass spectrometry and co-immunoprecipitation analysis demonstrated that Mon1a interacts with the microtubule-based motor Dynein, a protein known to be required in ER-Golgi trafficking. Both Mon1a and Dynein were found in the same vesicle fractions after differential centrifugation. Further, using a cell culture-based vesicle budding protocol adapted from the Schekman group, Mon1a silencing was shown to significantly inhibit the formation of ER-derived vesicles, ultimately disrupting anterograde transport (16). These data support a model where Mon1a is recruited to the ER surface to aid in vesicle formation. Dynein subsequently interacts with Mon1a to transport the vesicle from the ER to the Golgi apparatus, resulting in efficient anterograde trafficking.

4.2 Organelle maintenance

The Golgi apparatus is the hub of endomembrane membrane traffic where the endocytic and biosynthetic pathways converge (3,5,12,23). Newly synthesized proteins and lipids reach their appropriate destinations through highly regulated membrane trafficking networks that ensure the identity and fidelity of the endomembrane system. The content of the second chapter defines a role for Mon1a in early anterograde trafficking through an interaction with cytoplasmic Dynein that results in efficient ER-

Golgi transport of ER-derived vesicles (16). Protein depletion of Mon1a or Dynein by RNAi inhibits ER-Golgi trafficking; however, silencing of Dynein results in complete fragmentation of the Golgi apparatus. Disruption of trafficking at the ER-Golgi interface usually has dramatic effects on Golgi morphology as when tether proteins are suppressed by siRNA (24,25,27).

RNAi studies and protein interaction analysis in cell culture were used to characterize Mon1a activity in membrane traffic and organelle maintenance in the secretory pathway in the third chapter. A yeast two-hybrid screen found that Mon1a interacts with a F-BAR domain-containing protein FCHo2 that has been described to function in trafficking at the cell surface in clathrin-mediated endocytosis (28-32). The interaction between Mon1a and FCHo2 was confirmed by co-immunoprecipitation studies, yet whether this interaction is direct or indirect is not clear. Notably, the Golgi fragments in cells depleted for FCHo2 by RNAi. Therefore, new siRNA's targeting Mon1a were created to address the discrepancy in phenotypes between Mon1a and its interacting partners. siRNAs targeting the 5'-UTR of the Mon1a gene resulted in a fragmented Golgi phenotype strikingly similar to FCHo2 silenced cells. Further, the fragmented Golgi phenotypes required the activity of the Golgi GTPase Rab6 as co-silencing suppressed fragmentation, suggesting that Rab6 function is epistatic to both Mon1a and FCHo2.

FCHo2 is a member of a large family of proteins named after a conserved domain that defines the family, the F-BAR domain (28-32). In Chapter 3, we describe a novel function for FCHo2 at the Golgi apparatus in the formation of Golgi ribbons following mitotic events. Mammalian Golgi are unique in that they must be systematically broken

down into individual stacks and ultimately vesiculated to allow Golgi material to be allocated between the daughter cells (13,23,27,34-36). After mitosis, the Golgi is reassembled into mini-stacks that are laterally fused to create Golgi ribbons, presumably a membrane tubulating activity. Consequently, cells overexpressing F-BAR domain proteins, including FCHo2, have extensive membrane tubulation (28-30). We therefore hypothesized that after mitosis, FCHo2 is required to create Golgi ribbons, which laterally link individual stacks. The cell cycle was arrested in silenced cells preventing mitotically induced Golgi fragmentation, which tested our model. The data confirmed our hypothesis as cell cycle arrest suppressed Golgi fragmentation in FCHo2-depleted cells. Further, FRAP analysis demonstrated that FCHo2 is needed for lateral diffusion of Golgi material as photobleached Golgi regions were unable to recover fluorescence providing evidence of FCHo2's role in Golgi ribbon formation.

These data suggest that FCHo2 and Mon1a activity are required for maintenance of Golgi architecture. Mon1a and FCHo2 siRNA phenotypes are similar but not identical as both fragment the Golgi and require the activity of the Golgi GTPase Rab6. Golgi fragmentation in FCHo2-silenced cells, however, is cell cycle-dependent where the Mon1a phenotype is not. We have yet to identify FCHo2 at the Golgi ribbon, which we believe to be a transient interaction that is cell cycle-regulated. FCHo2 is recruited to the cell surface through an association with Ptd(4,5)P(2) (31). This novel role for FCHo2 in Golgi ribbon formation does not conflict with the identified activity of FCHo2 at the cell surface in endocytosis and perhaps Ptd(4,5)P(2) mediates recruitment of FCHo2 to Golgi cisternae to aid in ribbon formation. Studies are ongoing to clarify the biochemical functions of Mon1a and FCHo2 in Golgi maintenance and membrane trafficking.

4.3 Future directions

Our data have identified roles for Mon1a and FCHo2 in membrane traffic and Golgi maintenance, but more work is needed to understand the mechanisms of these actions (16). During the course of this work, several interesting results emerged that could provide critical insight into the mechanistic functions of Mon1a and FCHo2 in mammalian cells.

4.4 Mitochondrial maintenance in FCHo2-depleted cells

The Golgi complex is systemically broken down in mammalian cells as they enter mitosis to aid the dispersal of Golgi material between daughter cells (35-39). Another tubular organelle that follows a cell cycle-regulated breakdown and reassembly is the mitochondria (40-44). These morphological similarities in the Golgi and mitochondria prompted us to examine the structural status of mitochondria in FCHo2-silenced cells. Mitochondria were visibly disrupted in cells depleted of FCHo2, which demonstrated a role for FCHo2 in the maintenance of both mitochondria and Golgi architecture (**Figure 4.1**). Our data demonstrated that Golgi fragmentation in FCHo2-depleted cells is cell cycle- and Rab6-dependent. Whether the FCHo2 silencing-induced mitochondria phenotype is cell cycle- or Rab6-regulated remains to be demonstrated. Further, the functional significance of the Mon1a-FCHo2 interaction in Golgi and/or mitochondrial maintenance remains to be demonstrated. Currently, we are using protein truncations of Mon1a to map the FCHo2-binding domain so that RNAi and rescue studies can be performed to address the functional significance of this interaction in membrane traffic and organelle maintenance. Finally, intracellular localization of both Mon1a and FCHo2

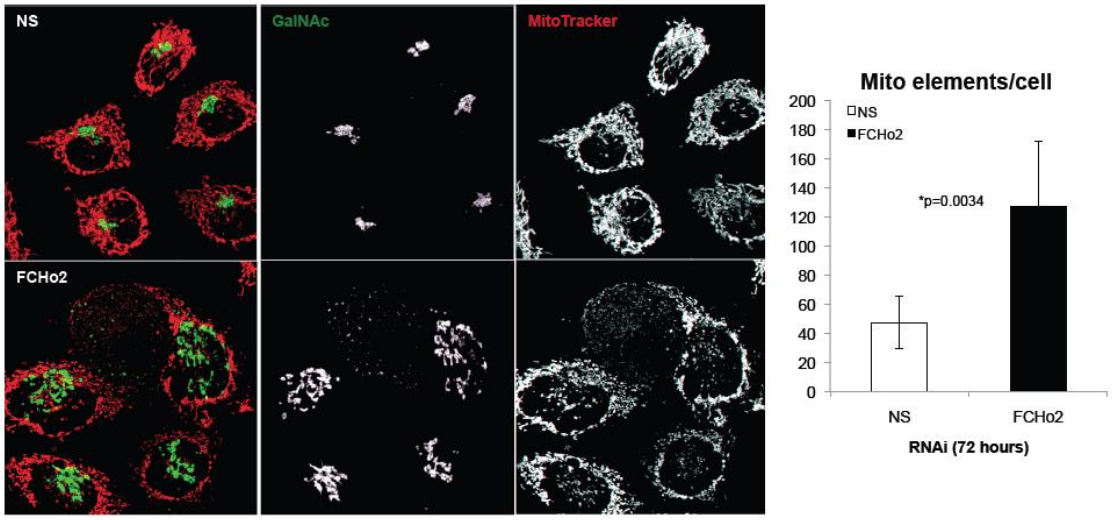

Figure 4.1 FCHo2 silencing fragments mitochondria Confocal images of nonspecifically and FCHo2 silenced GA=alNAc-T2-GFP expressing cells treated with MitoTracker. Quantification of mitochondria fragmentation was done over three independent experiments.

has been unsatisfactory. Subcellular localization studies in synchronized cells may be required to capture the likely transient interactions of Mon1a and FCHo2 at these organelles.

4.5 Golgi-ER retrograde trafficking

We demonstrated that Mon1a is required for anterograde trafficking to the Golgi. These data were discussed in Chapter 2. Subsequently, we have confirmed this result independently using co-silencing to demonstrate epistatic relationship between proteins involved in ER-Golgi transport. Golgi morphology was assessed in cells depleted of both Mon1a and the *cis*-Golgi tether p115 required in anterograde transport. It has been reported in the literature that siRNA-dependent silencing of p115 fragments the Golgi due to lack of tethering activity at the Golgi. Mon1a functions upstream of p115 at the ER in vesicle formation, a step required in anterograde trafficking. Co-depletion of

Mon1a and p115 suppressed Golgi fragmentation (**Figure 4.2**) providing further evidence for Mon1a function in Golgi-ER transport as well as acting as a positive control for these epistasis experiments.

We next considered whether Mon1a is involved in the reciprocal retrograde pathway. Both Mon1a and Rab6 recruit and interact with the motor Dynein to efficiently traffic vesicles to the appropriate organelle (15,16,27). One hypothesis follows that Mon1a is needed at the Golgi to aid in Rab6-dependent retrograde Golgi-ER trafficking and it would follow that Mon1a silencing might suppress ZW10 knockdown-dependent Golgi fragmentation. To address this possibility and determine the epistatic relationship of Mon1a and ZW10, co-silencing experiments were performed. RNAi targeting Mon1a (ORF) significantly depletes Mon1a protein but leaves Golgi morphology intact (16). It is thought that Golgi fragmentation in ZW10-silenced cells is a result of Rab6-dependent retrograde transport of Golgi-derived vesicles and subsequent lack of tethering activity at the ER, similar to p115 at the Golgi (27). Inhibiting retrograde transport upstream at the Golgi by depleting cells of Rab6 and subsequent vesicle formation suppresses the fragmented phenotype. Mon1a is required for anterograde transport at the ER in vesicle formation similar to Rab6 activity at the Golgi (16). Co-silencing of Mon1a and ZW10 also suppressed ZW10 knockdown-dependent Golgi fragmentation (**Figure 4.2**). We conclude from these data that Mon1a and Rab6 activity is required for Golgi fragmentation seen in ZW10-depleted cells. These data suggest a role for Mon1a in Rab6-dependent retrograde trafficking.

Functional data, however, are required to demonstrate that Mon1a is required in this Rab6-dependent retrograde pathway. Cholera toxin subunit B (CTxB) binds the cell

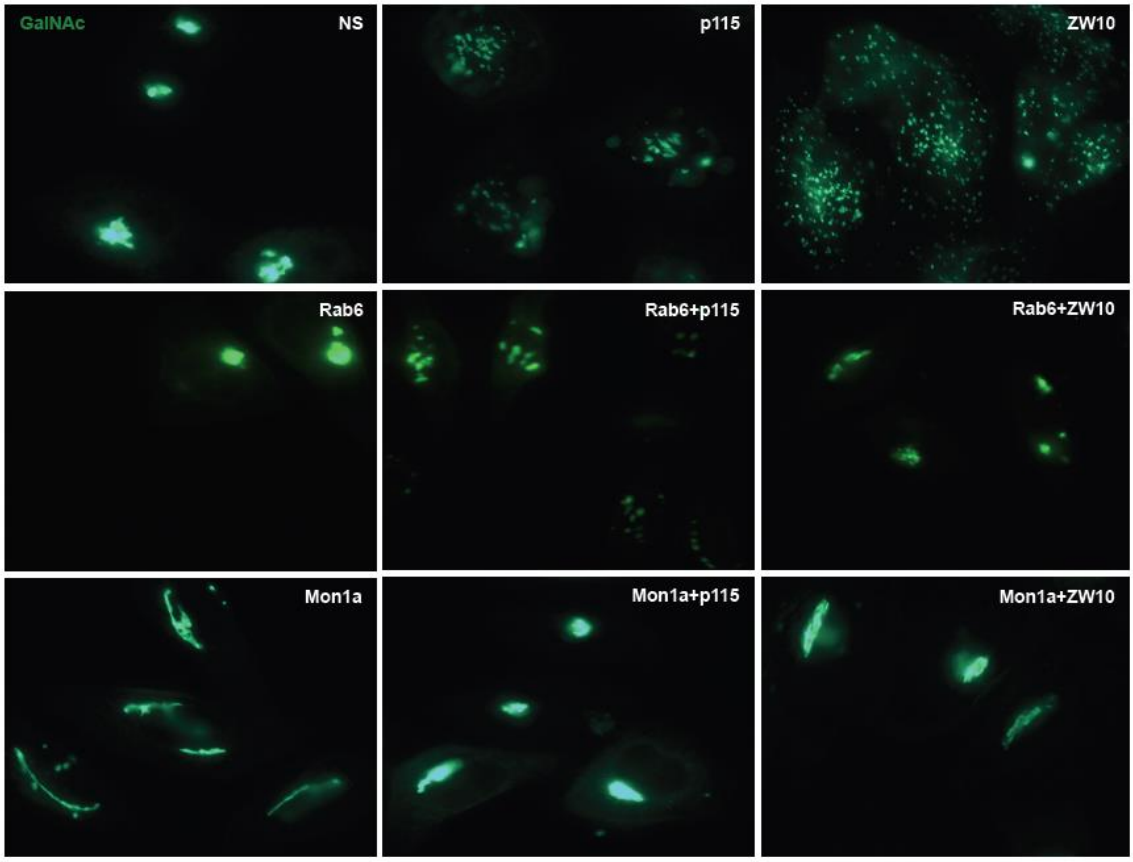

Figure 4.2 Co-silencing of Mon1a and tethers suppresses Golgi fragmentation GalNAc-T2-GFP-expressing cells were transfected with siRNAs to Rab6, Mon1a, p115, and ZW10 alone and in combination and Golgi morphology was assessed by epifluorescence microscopy.

surface, is internalized, and traffics to the ER via the Golgi apparatus traversing the entire retrograde pathway (45-48). Use of fluorophore-tagged CTxB in Mon1a-depleted cells will address the role of Mon1a in Rab6-dependent retrograde transport. Further, a role for FCHo2 in retrograde trafficking at the Golgi apparatus has yet to be addressed. Vesicle formation at the cell surface (towards the cytoplasm) where FCHo2 was originally described to function is topographically similar to vesicle budding at the Golgi. FCHo2 activity in retrograde transport can be addressed using RNAi analysis and CTxB trafficking.

4.6 Consequences of the allelic status of Mon1a

Mon1a was originally identified in mice in a quantitative trait locus (QTL) analysis that identified modifiers of the iron overload disorder hemochromatosis (22). That work identified a missense mutation in the Mon1a gene in C57BL mice that resulted in a "gain-of-function" allele that was capable of moving proteins through the secretory pathway more efficiently. Increased Mon1a activity in C57BL mice resulted in increased cell surface ferroportin levels and subsequent cellular and splenic iron reduction. To address the "gain-of-function" allele *ex vivo,* interlukin-12 (IL-12) levels were measured from splenocytes treated with LPS isolated from different strains of mice. Splenocytes from C57BL/6 mice showed significantly increased IL-12 secretion at all time points measured compared to the other strains (**Figure 4.3**). SWR and congenic mice with a wild type allele of Mon1a secreted less IL-12 than C57BL/6 mice demonstrating "gain-of-function" activity of this allele. The allelic status of Mon1a could have significant ramifications on several biological processes, including the inflammatory response and pathogen clearance. Characterizing Mon1a in disease models could yield important insights to our understanding of membrane traffic in disease progression. Protein interaction studies comparing the binding partners of the Mon1a alleles could identify protein partners specific to an allele of Mon1a that could help us understand the biochemical mechanism of Mon1a function.

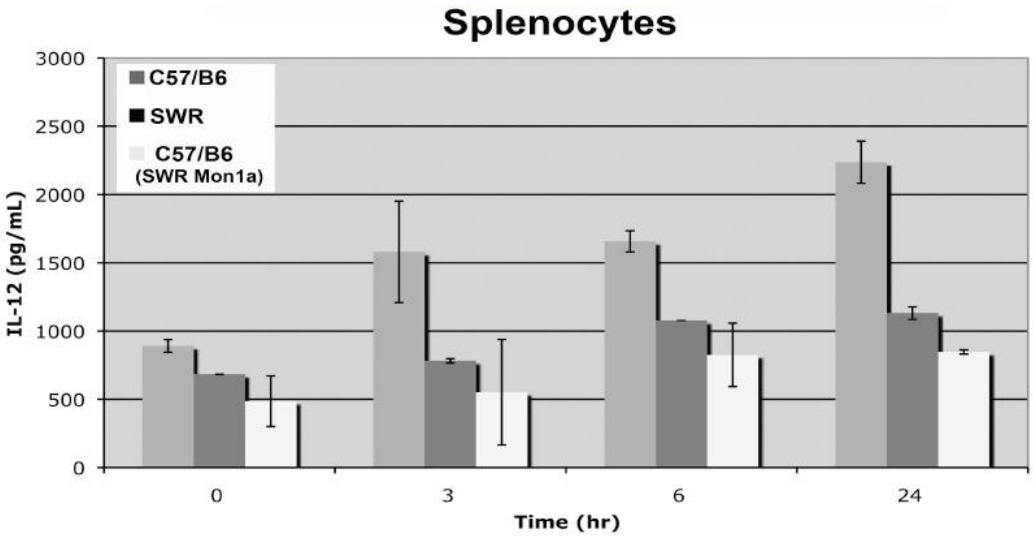

Figure 4.3 In vivo analysis of cytokine secretion in LPS treated splenocytes Splenocytes isolated from mice were treated with LPS and IL-12 analysis was determined by ELISA at indicated time points.

4.7 References

1. Brighouse, A., Dacks, J. B., and Field, M. C. 2010 *Cell Mol Life Sci* 67: 3449-3465

2. Dacks, J. B., and Field, M. C. 2007 *J Cell Sci* 120: 2977-2985

3. Gurkan, C., Koulov, A. V., and Balch, W. E. 2007 *Adv Exp Med Biol* 607: 73-83

4. Jamieson, J. D., and Palade, G. E. 1967 *J Cell Biol* 34: 597-615

5. Lippincott-Schwartz, J., and Phair, R. D. 2010 *Annu Rev Biophys* 39: 559-578

6. Mellman, I., and Warren, G. 2000 *Cell* 100: 99-112

7. Schekman, R. 2010 *Mol Biol Cell* 21: 3781-3784

8. Vellai, T., and Vida, G. 1999 *Proc Biol Sci* 266: 1571-1577

9. Novick, P., Ferro, S., and Schekman, R. 1981 *Cell* 25: 461-469

10. Novick, P., Field, C., and Schekman, R. 1980 *Cell* 21: 205-215

11. Novick, P., and Schekman, R. 1979 *Proc Natl Acad Sci U S A* 76: 1858-1862

12. Vinke, F. P., Grieve, A. G., and Rabouille, C. 2011 *Biochem J* 433: 423-433

13. Jamieson, J. D., and Palade, G. E. 1966 *Proc Natl Acad Sci U S A* 55: 424-431

14. Kellokumpu, S., Sormunen, R., and Kellokumpu, I. 2002 *FEBS Lett* 516: 217-224

15. Matanis, T., Akhmanova, A., Wulf, P., Del Nery, E., Weide, T., Stepanova, T., Galjart, N., Grosveld, F., Goud, B., De Zeeuw, C. I., Barnekow, A., and Hoogenraad, C. C. 2002 *Nat Cell Biol* 4: 986-992

16. Bagley, D. C., Paradkar, P. N., Kaplan, J., and Ward, D. M. 2012 *The Journal of biological chemistry* 287: 25577-25588

17. Kinchen, J. M., and Ravichandran, K. S. 2010 *Nature* 464: 778-782

18. Poteryaev, D., Datta, S., Ackema, K., Zerial, M., and Spang, A. 2010 *Cell* 141: 497-508

19. Poteryaev, D., Fares, H., Bowerman, B., and Spang, A. 2007 *EMBO J* 26: 301-312

20. Wang, C. W., Stromhaug, P. E., Kauffman, E. J., Weisman, L. S., and Klionsky, D. J. 2003 *J Cell Biol* 163: 973-985

21. Wang, C. W., Stromhaug, P. E., Shima, J., and Klionsky, D. J. 2002 *J Biol Chem* 277: 47917-47927

22. Wang, F., Paradkar, P. N., Custodio, A. O., McVey Ward, D., Fleming, M. D., Campagna, D., Roberts, K. A., Boyartchuk, V., Dietrich, W. F., Kaplan, J., and Andrews, N. C. 2007 *Nat Genet* 39: 1025-1032

23. Wang, Y., and Seemann, J. 2011 *Cold Spring Harb Perspect Biol* 3: a005330

24. Puthenveedu, M. A., and Linstedt, A. D. 2001 *J Cell Biol* 155: 227-238

25. Puthenveedu, M. A., and Linstedt, A. D. 2004 *Proc Natl Acad Sci U S A* 101: 1253-1256

26. Seemann, J., Jokitalo, E. J., and Warren, G. 2000 *Mol Biol Cell* 11: 635-645
27. Sun, Y., Shestakova, A., Hunt, L., Sehgal, S., Lupashin, V., and Storrie, B. 2007 *Mol Biol Cell* 18: 4129-4142

28. Frost, A., De Camilli, P., and Unger, V. M. 2007 *Structure* 15: 751-753

29. Frost, A., Perera, R., Roux, A., Spasov, K., Destaing, O., Egelman, E. H., De Camilli, P., and Unger, V. M. 2008 *Cell* 132: 807-817

30. Frost, A., Unger, V. M., and De Camilli, P. 2009 *Cell* 137: 191-196

31. Henne, W. M., Boucrot, E., Meinecke, M., Evergren, E., Vallis, Y., Mittal, R., and McMahon, H. T. 2010 *Science* 328: 1281-1284

32. Henne, W. M., Kent, H. M., Ford, M. G., Hegde, B. G., Daumke, O., Butler, P. J., Mittal, R., Langen, R., Evans, P. R., and McMahon, H. T. 2007 *Structure* 15: 839-852

33. Futterer, K., and Machesky, L. M. 2007 *Cell* 129: 655-657

34. Del Nery, E., Miserey-Lenkei, S., Falguieres, T., Nizak, C., Johannes, L., Perez, F., and Goud, B. 2006 *Traffic* 7: 394-407

35. Feinstein, T. N., and Linstedt, A. D. 2008 *Mol Biol Cell* 19: 2696-2707

36. Tang, D., and Wang, Y. 2013 *Trends Cell Biol*

37. Tang, D., Xiang, Y., and Wang, Y. 2010 *Nat Protoc* 5: 758-772

38. Tang, D., Yuan, H., Vielemeyer, O., Perez, F., and Wang, Y. 2012 *Biol Open* 1: 1204-1214

39. Tang, D., Yuan, H., and Wang, Y. 2010 *Traffic* 11: 827-842

40. Westermann, B. 2002 *EMBO Rep* 3: 527-531

41. Mozdy, A. D., and Shaw, J. M. 2003 *Nat Rev Mol Cell Biol* 4: 468-478

42. Kashatus, D. F., Lim, K. H., Brady, D. C., Pershing, N. L., Cox, A. D., and Counter, C. M. 2011 *Nat Cell Biol* 13: 1108-1115

43. Taguchi, N., Ishihara, N., Jofuku, A., Oka, T., and Mihara, K. 2007 *J Biol Chem* 282: 11521-11529

44. Horn, S. R., Thomenius, M. J., Johnson, E. S., Freel, C. D., Wu, J. Q., Coloff, J. L., Yang, C. S., Tang, W., An, J., Ilkayeva, O. R., Rathmell, J. C., Newgard, C. B., and Kornbluth, S. 2011 *Mol Biol Cell* 22: 1207-1216

45. Sandvig, K., and van Deurs, B. 2002 *FEBS Lett* 529: 49-53

46. Lencer, W. I., and Tsai, B. 2003 *Trends Biochem Sci* 28: 639-645

47. Johannes, L., and Goud, B. 1998 *Trends Cell Biol* 8: 158-162

48. White, J., Johannes, L., Mallard, F., Girod, A., Grill, S., Reinsch, S., Keller, P., Tzschaschel, B., Echard, A., Goud, B., and Stelzer, E. H. 1999 *J Cell Biol* 147: 743-760